Novel Green Synthesis of Polyfunctionally Substituted Phthalazines Promoted by Visible Light, DFT Studies and Molecular Docking with Antimicrobial and Antibiofilm Potency

Ramadan A. Mekheimer, Basma A. Khalifa, Zeinab Shawky Hashem, Samar M. R. Allam, Kamal Usef Sadek, Mohamed R. Eletmany

Contents

1. Methodology

1.1. General Equation

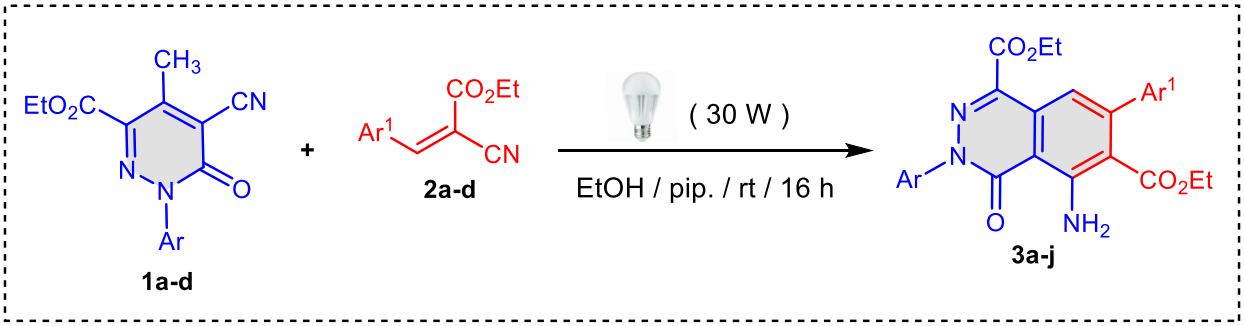

Diethyl 5-amino-3,7-bis(4-chlorophenyl)-4-oxo-3,4-dihydrophthalazine-1,6-dicarboxylate (3a).

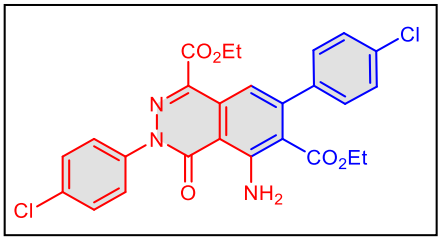

Yellow crystals; yield (93%); mp: 238-240°C. IR (KBr): ν = 3452, 3328 (NH_2), 2960 (aliph. CH), 1720, 1704 (ester C=O) cm^{-1}. ^1H NMR (400 MHz): δ_H = 0.76 (t, 3H, J = 7.2 Hz, CH_3), 1.29 (t, 3H, J = 7.2 Hz, CH_3), 4.0 (q, 2H, J = 7.2 Hz, CH_2), 4.36 (q, 2H, J = 7.2 Hz, CH_2), 7.34 (d, J = 8.8 Hz, 2 Ar-H), 7.40 (s, 1 Ar-H), 7.56 (d, J = 8.4 Hz, 2 Ar-H), 7.60-7.66 (m, 4 Ar-H), 7.98 (br, 2H, NH_2). ^{13}C NMR (100 MHz): δ_C = 13.08 (CH_3), 13.91 (CH_3), 60.94 (CH_2), 61.93 (CH_2), 110.20 (C-6), 112.35 (C-4a), 115.25 (C-8), 128.34 (2 Ar-C), 128.48 (2 Ar-C), 128.75 (2 Ar-C), 129.38 (2 Ar-C), 129.84 (1 Ar-C), 132.73 (1 Ar-C), 132.98 (1 Ar-C), 136.61 (C-1), 139.68 (C-7), 139.78 (1 Ar-C), 146.74 (C-8a), 149.90 (C-5), 160.34 (C-4), 162.58 (C=O), 166.87 (C=O). MS: (EI) m/z %: 526 (M^+, 100), 451 (9), 372 (14), 302 (5), 282 (32), 256 (21), 199 (14), 111 (45). Anal. Calcd. for $C_{26}H_{21}Cl_2N_3O_5$ (526.37): C, 59.33; H, 4.02; Cl, 13.47; N, 7.98%; Found: C, 59.44; H, 4.17; Cl, 13.37; N, 8.05%.

Diethyl 5-amino-3-(4-chlorophenyl)-7-(4-nitrophenyl)-4-oxo-3,4-dihydrophthalazine-1,6-dicarboxylate (3b).

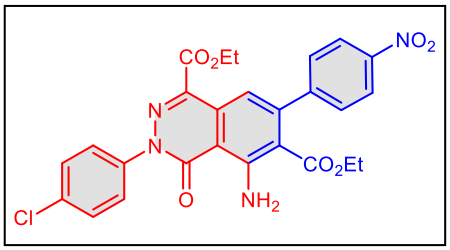

Pale yellow crystals; yield (92%); mp: 225-227°C. IR (KBr): ν = 3456, 3324 (NH_2), 3108 (arom. CH), 2984 (aliph. CH), 1728, 1701 (ester C=O) cm^{-1}. ^1H NMR (600 MHz): δ_H = 0.76 (t, 3H, J = 6.0 Hz, CH_3), 1.29 (t, 3H, J = 6.0 Hz, CH_3), 3.97 (q, 2H, J = 6.0 Hz, CH_2), 4.36 (q, 2H, J = 6.0 Hz, CH_2), 7.43 (s, 1 Ar-H), 7.60-7.66 (m, 6 Ar-H), 8.16 (br, 2H, NH_2), 8.34 (d, J = 8.4 Hz, 2 Ar-H).

^{13}C NMR (150 MHz): δ_C = 13.51 (CH_3), 14.41 (CH_3), 61.57 (CH_2), 62.47 (CH_2), 111.39 (C-6), 112.78 (C-4a), 114.49 (C-8), 124.08 (2 Ar-C), 128.83 (2 Ar-C), 129.27 (2 Ar-C), 129.49 (2 Ar-C), 130.65 (1 Ar-C), 133.31 (1 Ar-C), 136.86 (C-1), 140.24 (C-7), 146.78 (C-8a), 147.52 (1 Ar-C), 148.33 (1 Ar-C), 150.92 (C-5), 160.80 (C-4), 163.03 (C=O), 167.03 (C=O). Anal. Calcd. for $C_{26}H_{21}ClN_4O_7$ (536.93): C, 58.16; H, 3.94; Cl, 6.60; N, 10.43%; Found: C, 58.03; H, 4.05; Cl, 6.50; N, 10.60%.

Diethyl 5-amino-7-(4-chlorophenyl)-4-oxo-3-(p-tolyl)-3,4-dihydrophthalazine-1,6-dicarboxylate

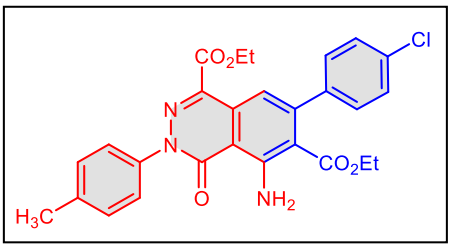

(3c). Yellow crystals; yield (91%); mp: 230-232°C. IR (KBr): *v* = 3422, 3304 (NH_2), 3148 (arom. CH), 2982 (aliph. CH), 1707 (ester C=O), 1645 (amide C=O) cm^{-1}. ^{1}H NMR (600 MHz): δ_H = 0.82 (t, 3H, *J* = 6.0 Hz, CH_3), 1.28 (t, 3H, *J* = 6.0 Hz, CH_3), 2.40 (s, 3H, CH_3), 3.99 (q, 2H, *J* = 6.0 Hz, CH_2), 4.36 (q, 2H, *J* = 6.0 Hz, CH_2), 7.34-7.36 (m, 4 Ar-H), 7.41 (s, 1 Ar-H), 7.46 (d, 2H, *J* = 6.0 Hz, Ar-H), 7.56 (d, 2H, *J* = 6.0 Hz, Ar-H), 8.0 (br, 2H, NH_2). ^{13}C NMR (150 MHz): δ_C = 13.58 (CH_3), 14.42 (CH_3), 21.21 (CH_3), 61.41 (CH_2), 62.36 (CH_2), 110.82 (C-6), 112.75 (C-4a), 115.39 (C-8), 126.82 (2 Ar-C), 128.92 (1 Ar-C), 129.69 (2 Ar-C), 129.89 (1 Ar-C), 130.42 (1 Ar-C), 130.84 (1 Ar-C), 133.44 (1 Ar-C), 136.67 (C-1), 138.45 (1 Ar-C), 139.11 (C-7), 140.29 (C-8a), 147.19 (1 Ar-C), 150.45 (1 Ar-C), 151.17 (C-5), 163.19 (C-4), 164.23 (C=O), 167.43 (C=O). Anal. Calcd. for $C_{27}H_{24}ClN_3O_5$ (505.96): C, 64.10; H, 4.78; Cl, 7.01; N, 8.31%; Found: C, 64.17; H, 4.91; Cl, 7.10; N, 8.25%.

Diethyl 5-amino-7-(3-nitrophenyl)-4-oxo-3-(p-tolyl)-3,4-dihydrophthalazine-1,6-dicarboxylate

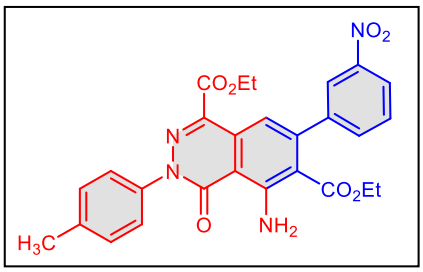

(3d). Yellow crystals; yield (90%); mp: 238-240°C. IR (KBr): *v* = 3423, 3304 (NH_2), 3149 (arom. CH), 2983 (aliph. CH), 1708 (ester C=O), 1645 (amide C=O) cm^{-1}. ^{1}H NMR (400 MHz): δ_H = 0.82 (t, 3H, *J* = 6.8 Hz, CH_3), 1.29 (t, 3H, *J* = 7.2 Hz, CH_3), 2.40 (s, 3H, CH_3), 3.99 (q, 2H, *J* = 7.2 Hz, CH_2), 4.36 (q, 2H, *J* = 7.2 Hz, CH_2), 7.34 (d, 2H, *J* = 8.8 Hz, Ar-H), 7.40 (s, 1H, Ar-H), 7.56 (d, 2H, *J* = 8.8 Hz, Ar-H), 7.60-7.65 (m, 4 Ar-H), 7.97 (s, 2H, NH_2). Anal. Calcd for $C_{27}H_{24}N_4O_7$: C, 62.79; H, 4.68; N, 10.85%; Found: C, 62.91; H, 4.51; N, 11.00%.

Diethyl 5-amino-7-(4-fluorophenyl)-4-oxo-3-(p-tolyl)-3,4-dihydrophthalazine-1,6-dicarboxylate

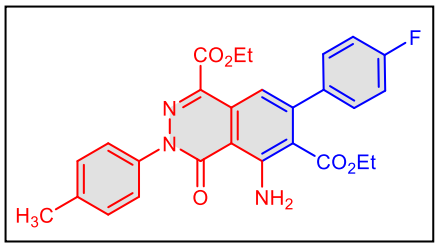

(3e). Yellow crystals; yield (90%); mp: 218-220°C. IR (KBr): *v* = 3421, 3304 (NH_2), 3148 (arom. CH), 2982 (aliph. CH), 1708 (ester C=O), 1644 (amide C=O) cm^{-1}. ^1H NMR (600 MHz): δ_H = 0.81 (t, 3H, *J* = 6.0 Hz, CH_3), 1.28 (t, 3H, *J* = 6.0 Hz, CH_3), 2.40 (s, 3H, CH_3), 3.99 (q, 2H, *J* = 6.0 Hz, CH_2), 4.36 (q, 2H, *J* = 6.0 Hz, CH_2), 7.34-7.36 (m, 4 Ar-H), 7.41 (s, 1 Ar-H), 7.46 (d, 2H, *J* = 6.0 Hz, Ar-H), 7.56 (d, 2H, *J* = 6.0 Hz, Ar-H), 8.0 (br, 2H, NH_2). Anal. Calcd. for $C_{27}H_{24}FN_3O_5$ (489.50): C, 66.25; H, 4.94; F, 3.88; N, 8.58%; Found: C, 66.19; H, 5.02; F, 3.77; N, 8.70%.

Diethyl 5-amino-3-(2-chlorophenyl)-7-(4-chlorophenyl)-4-oxo-3,4-dihydrophthalazine-1,6-dicarboxylate

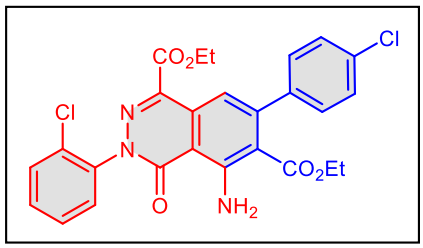

(3f). Yellow crystals; yield (92%); mp: 235-237°C. IR (KBr): *v* = 3422, 3305 (NH_2), 3150 (arom. CH), 2982 (aliph. CH), 1708 (ester C=O), 1644 (amide C=O) cm^{-1}. ^1H NMR (600 MHz): δ_H = 0.83 (t, 3H, *J* = 6.0 Hz, CH_3), 1.28 (t, 3H, *J* = 6.0 Hz, CH_3), 4.01 (q, 2H, *J* = 6.0 Hz, CH_2), 4.36 (q, 2H, *J* = 6.0 Hz, CH_2), 7.37 (d, 2H, *J* = 8.0 Hz, Ar-H), 7.42 (s, 1 Ar-H), 7.46-7.58 (m, 4 Ar-H), 7.72 (s, 2 Ar-H), 7.93 (br, 2H, NH_2). Anal. Calcd. for $C_{26}H_{21}Cl_2N_3O_5$ (526.37): C, 59.33; H, 4.02; Cl, 13.47; N, 7.98%; Found: C, 59.25; H, 4.14; Cl, 13.60; N, 7.92%.

Diethyl 5-amino-3-(2-chlorophenyl)-7-(4-fluorophenyl)-4-oxo-3,4-dihydrophthalazine-1,6-dicarboxylate

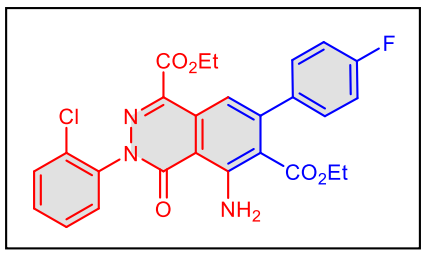

(3g). Yellow crystals; yield (90%); mp: 248-250°C. IR (KBr): *v* = 3454, 3332 (NH_2), 2997, 2902 (aliph. CH), 1722 (ester C=O), 1708 (ester C=O), 1682 (amide C=O) cm^{-1}. ^1H NMR (600 MHz): δ_H = 0.77 (t, 3H, *J* = 6.0 Hz, CH_3), 1.27 (t, 3H, *J* = 6.0 Hz, CH_3), 3.98 (q, 2H, *J* = 6.0 Hz, CH_2), 4.35 (q, 2H, *J* = 6.0 Hz, CH_2), 7.46 (s, 1 Ar-H), 7.58-7.60 (m, 2 Ar-H), 7.64 (d, 2H, *J* = 6.0 Hz, Ar-H), 7.72-7.74 (m, 2 Ar-H), 8.13 (br, 2H, NH_2), 8.35 (d, 2H, *J* = 12.0 Hz, Ar-H). ^{13}C NMR (150 MHz): δ_C = 13.53 (CH_3), 14.39 (CH_3), 61.56 (CH_2), 62.60 (CH_2), 110.92 (C-6), 113.12 (C-4a), 114.94 (C-8), 124.11 (3 Ar-C), 128.92 (1 Ar-C), 129.53 (2 Ar-C), 130.43 (1 Ar-C), 130.62 (1 Ar-C), 131.48 (1 Ar-C), 131.61 (1 Ar-C), 137.35 (C-1), 138.87 (C-7), 147.02 (1 Ar-C), 147.58 (C-8a), 148.24 (1 Ar-C), 150.77 (C-5), 160.52

(C-4), 162.87 (C=O), 166.90 (C=O). Anal. Calcd. for $C_{26}H_{21}ClFN_3O_5$ (509.92): C, 61.24; H, 4.15; Cl, 6.95; F, 3.73; N, 8.24%; Found: C, 61.15; H, 4.31; Cl, 6.85; F, 3.61; N, 8.17%.

Diethyl 5-amino-7-(4-chlorophenyl)-4-oxo-3-phenyl-3,4-dihydrophthalazine-1,6-dicarboxylate

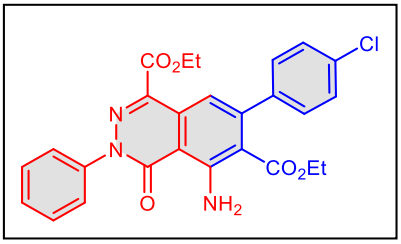

(3h). Yellow crystals; yield (90%); mp: 222-224°C. IR (KBr): *v* = 3459, 3334 (NH_2), 2991 (aliph. CH), 1722 (ester C=O), 1705 (ester C=O), 1644 (amide C=O) cm^{-1}. ^1H NMR (600 MHz): δ_H = 0.82 (t, 3H, *J* = 6.0 Hz, CH_3), 1.29 (t, 3H, *J* = 6.0 Hz, CH_3), 4.0 (q, 2H, *J* = 6.0 Hz, CH_2), 4.36 (q, 2H, *J* = 6.0 Hz, CH_2), 7.35 (d, 2H, *J* = 12.0 Hz, Ar-H), 7.42 (s, 1 Ar-H), 7.47-7.60 (m, 8H, 6 Ar-H and NH_2), 7.65 (d, 1H, *J* = 6.0 Hz, Ar-H). Anal. Calcd. for $C_{26}H_{22}ClN_3O_5$ (491.93): C, 63.48; H, 4.51; Cl, 7.21; N, 8.54%; Found: C, 63.38; H, 4.59; Cl, 7.08; N, 8.65%.

Diethyl 5-amino-7-(4-nitrophenyl)-4-oxo-3-phenyl-3,4-dihydrophthalazine-1,6-dicarboxylate

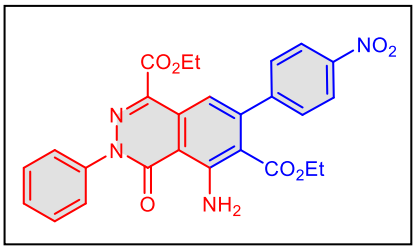

(3i). Pale yellow crystals; yield (93%); mp: 226-228°C. IR (KBr): *v* = 3422, 3305 (NH_2), 3150 (arom. CH), 2982 (aliph. CH), 1708 (ester, C=O), 1644 (amide C=O) cm^{-1}. ^1H NMR (600 MHz): δ_H = 0.76 (t, 3H, *J* = 6.0 Hz, CH_3), 1.28 (t, 3H, *J* = 6.0 Hz, CH_3), 3.98 (q, 2H, *J* = 6.0 Hz, CH_2), 4.36 (q, 2H, *J* = 6.0 Hz, CH_2), 7.45 (s, 1 Ar-H), 7.49 (s, 1 Ar-H), 7.55-7.62 (m, 8H, 6 Ar-H and NH_2), 8.35 (d, 2H, *J* = 6.0 Hz, 2 Ar-H). ^{13}C NMR (150 MHz): δ_C = 13.52 (CH_3), 14.42 (CH_3), 61.48 (CH_2), 62.43 (CH_2), 111.49 (C-6), 112.72 (C-4a), 114.30 (C-8), 124.09 (2 Ar-C), 127.06 (2 Ar-C), 128.95 (1 Ar-C), 129.30 (2 Ar-C), 129.50 (2 Ar-C), 130.72 (1 Ar-C), 136.58 (C-1), 141.49 (C-7), 146.71 (C-8a), 147.51 (1 Ar-C), 148.42 (1 Ar-C), 150.97 (C-5), 160.88 (C-4), 163.12 (C=O), 167.06 (C=O). Anal. Calcd. for $C_{26}H_{22}N_4O_7$ (502.48): C, 62.15; H, 4.41; N, 11.15%; Found: C, 62.24; H, 4.35; N, 11.29%.

Diethyl 5-amino-7-(3-nitrophenyl)-4-oxo-3-phenyl-3,4-dihydrophthalazine-1,6-dicarboxylate

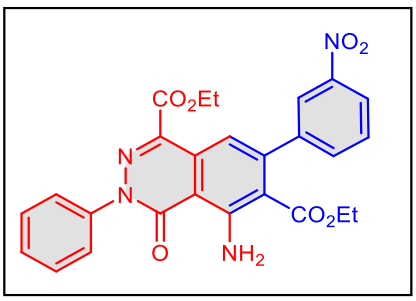

(3j). Yellow crystals; yield (93%); mp: 242-244°C. IR (KBr): *v* = 3423, 3317 (NH_2), 3100 (arom. CH), 1742 (ester, C=O), 1727 (ester, C=O) 1662 (amide C=O) cm^{-1}. ^1H NMR: δ_H = 0.82 (t, 3H, *J* = 6.0 Hz, CH_3), 1.29 (t, 3H, *J* = 6.0 Hz, CH_3), 3.99 (q, 2H, *J* = 6.0 Hz, CH_2), 4.36 (q, 2H, *J* = 6.0 Hz, CH_2), 7.34-7.36 (m, 4 Ar-H), 7.4

(s, 1 Ar-H), 7.46 (m, 2 Ar-H), 7.56 (d, 2H, *J* = 12 Hz, Ar-H), 7.66 (s, 1 Ar-H), 8.0 (br, 2H, NH_2). Anal. Calcd. for $C_{26}H_{22}N_4O_7$ (502.48): C, 62.15; H, 4.41; N, 11.15%. Found: C, 62.08; H, 4.54; N, 11.09%.

1.2. Antimicrobial screening

1.2.1. Microorganisms, Culture Conditions, and Compound Preparation

Antimicrobial testing was performed against clinically multi-resistant isolated strains of *S. aureus*, *K. pneumoniae*, *P. aeruginosa*, and *C. albicans*, obtained from the Microbiology Laboratory, Faculty of Pharmacy, Minia University. Bacterial strains were cultured in tryptic soy broth (TSB), and *C. albicans* was cultured in Sabouraud dextrose broth (SDB). Cultures were incubated at 37°C for 24 hours and adjusted to a 0.5 McFarland standard. A series of synthesized polyfunctionally substituted phthalazine derivatives **(3a-j)** were evaluated. Each compound was dissolved in dimethyl sulfoxide (DMSO) to prepare 2 mg/mL stock solutions and subsequently filtered using 0.22 µm filters. Working concentrations were prepared by serial dilution in sterile distilled water prior to testing.

1.2.2. Antimicrobial Susceptibility Testing

The agar well diffusion method was performed to assess the antimicrobial activity. Mueller-Hinton agar (MHA) plates for bacteria and Sabouraud dextrose agar (SDA) plates for fungi were inoculated with standardized microbial inocula. Six millimetres wells were punched and filled with 20 µL of each compound. Ciprofloxacin (20 µg/mL) and fluconazole (20 µg/mL) served as reference antibiotics for bacterial and fungal strains, respectively, while DMSO was used as a negative control. The plates were incubated overnight at 37°C, and inhibition zone diameters were measured.

1.2.3. Determination of Minimum Inhibitory Concentration (MIC) and Minimum Bactericidal/Fungicidal Concentration (MBC/MFC)

The Minimum Inhibitory Concentration (MIC) values were determined using the broth microdilution method. Two hundred microliters of each phthalazine derivative solutions were added to the first column of a 96-well microtiter plate, followed by serial two-fold dilutions across the row, resulting in final concentrations ranging from 200 to 0.82 µg/mL. Each well received 10 µL of bacterial or fungal inoculum suspension. Columns 11 and 12 served as microbial growth and broth sterility controls respectively. Plates were incubated at 37°C for 24 hours. The MIC was

defined as the lowest concentration of an antimicrobial agent that completely inhibits the visible growth of a microorganism. All data were reported as the mean of three independent experiments, each performed in duplicate. The Minimum Bactericidal and Fungicidal Concentrations (MBC and MFC) were determined polystyrene microplates by streaking samples from each MIC well onto agar plates. The lowest concentration at which no visible microbial growth was observed after incubation, indicating bactericidal or fungicidal activity.

1.2.4. Biofilm Inhibition Assay

The antibiofilm activity of the phthalazine compounds was investigated using the crystal violet staining method in 96-well flat-bottom [1]. Each well was loaded with 180 µL of TSB supplemented with 1% glucose, 10 µL of microbial inoculum, and 10 µL of test compound. Negative control wells received an equivalent volume of DMSO. Following static incubation at 37°C for 24 hours, non-adherent cells were removed by washing with phosphate-buffered saline (PBS, pH 7.2). Plates were air-dried and biofilms were fixed with 99% methanol for 15 minutes. Wells were then stained with 0.5% crystal violet for 30 minutes, washed with distilled water to remove excess stain, and air-dried. The bound dye was solubilized using 95% ethanol and absorbance was measured at 570 nm using a microplate reader.

The biofilm inhibition percentage was calculated using the following formula:

% Inhibition = [(OD control – OD treated) / OD control] × 100

All experiments were performed in triplicate and repeated independently three times.

1.3. Computational Methodology

1.3.1. DFT Strategy

Calculations were carried out using the 6-311G(d,p) basis set within the Gaussian 09 software suite [2]. Molecular electrostatic potential (MEP) mapping was performed to pinpoint key nucleophilic and electrophilic regions in the optimized structure. The most stable conformer and its electronic excitation properties were visualized using Chemcraft [3] and VMD [4] to elucidate its electronic characteristics. Harmonic vibrational frequencies computed at the 6-311G(d,p) level were scaled using a factor of 0.967, as recommended by NIST (https://cccbdb.nist.gov/vibscalejustx.asp) [5], to correct for anharmonic effects. ^{1}H and ^{13}C NMR spectra were computed using the Gauge-Including Atomic Orbital (GIAO) method within the DFT framework [6]. Time-Dependent Density Functional Theory (TD-DFT), a widely adopted

approach for simulating UV/vis absorption spectra and characterizing electronic excitation states in various molecular systems [7], was employed in this study. The TD-DFT calculations were conducted using the Conductor-like Polarizable Continuum Model (CPCM) to simulate solvent effects in DMSO.

Further topological analyses were executed using Multiwfn software [8], including reduced density gradient (RDG) and non-covalent interaction (NCI) analyses, alongside the electron localization function (ELF), to thoroughly characterize the intramolecular interactions and bonding nature within the heterocyclic framework [9].

The quantum chemical reactivity parameters for all the designed systems were computed following geometric optimization. These parameters were evaluated using the HOMO and LUMO energy values, based on the equations provided as the following [10,11].

$$\text{Energy Gap } (\Delta E) = E_{LUMO} - E_{HOMO} \quad (1)$$

$$\text{Ionization potential } (I) = - E_{HOMO} \quad (2)$$

$$\text{Electron affinity } (A) = - E_{LUMO} \quad (3)$$

$$\text{Hardness } (\eta) = (I-A)/2 \quad (4)$$

$$\text{Chemical potential } (\mu) = - (I+A)/2 \quad (5)$$

$$\text{Softness } (\sigma) = 1/ \eta \quad (6)$$

$$\text{Electronegativity } (\chi) = -(E_{HOMO} + E_{LUMO})/2 \quad (7)$$

$$\text{Electrophilicity } (\omega) = \mu^2/2\eta \quad (8)$$

1.3.2. Molecular Docking methodology

The molecular docking procedure followed a well-established protocol to ensure reliable and reproducible results [12,13]. Docking simulations for the investigated heterocyclic compounds were conducted using AutoDock Vina software [14]. Post-docking analysis and visualization of ligand–protein interactions were carried out using Discovery Studio (https://www.3ds.com/products-services/biovia/). The selected receptors S. aureus (ID:2XCT) [15] and human CYP51 (ID: 3LD6) [16] were obtained from the Protein Data Bank (https://www.rcsb.org/). Protein preparation involved the removal of water molecules and non-essential atoms, adding polar hydrogen atoms, and assigning partial atomic charges. The ligand and protein files were converted into the PDBQT format for docking. Active site coordinates were

determined, and a grid box was defined with dimensions of 40 × 40 × 40 Å and a grid spacing of 0.375 Å. The grid centers were set at coordinates (x = 21.348, y = 24.336, z = 79.243) for 2XCT and (x = 42.348, y = -0.623, z = -1.711) for 3LD6. The Genetic Algorithm (GA) was employed as the docking search method to predict optimal binding conformations [17].

2. Spectral Data

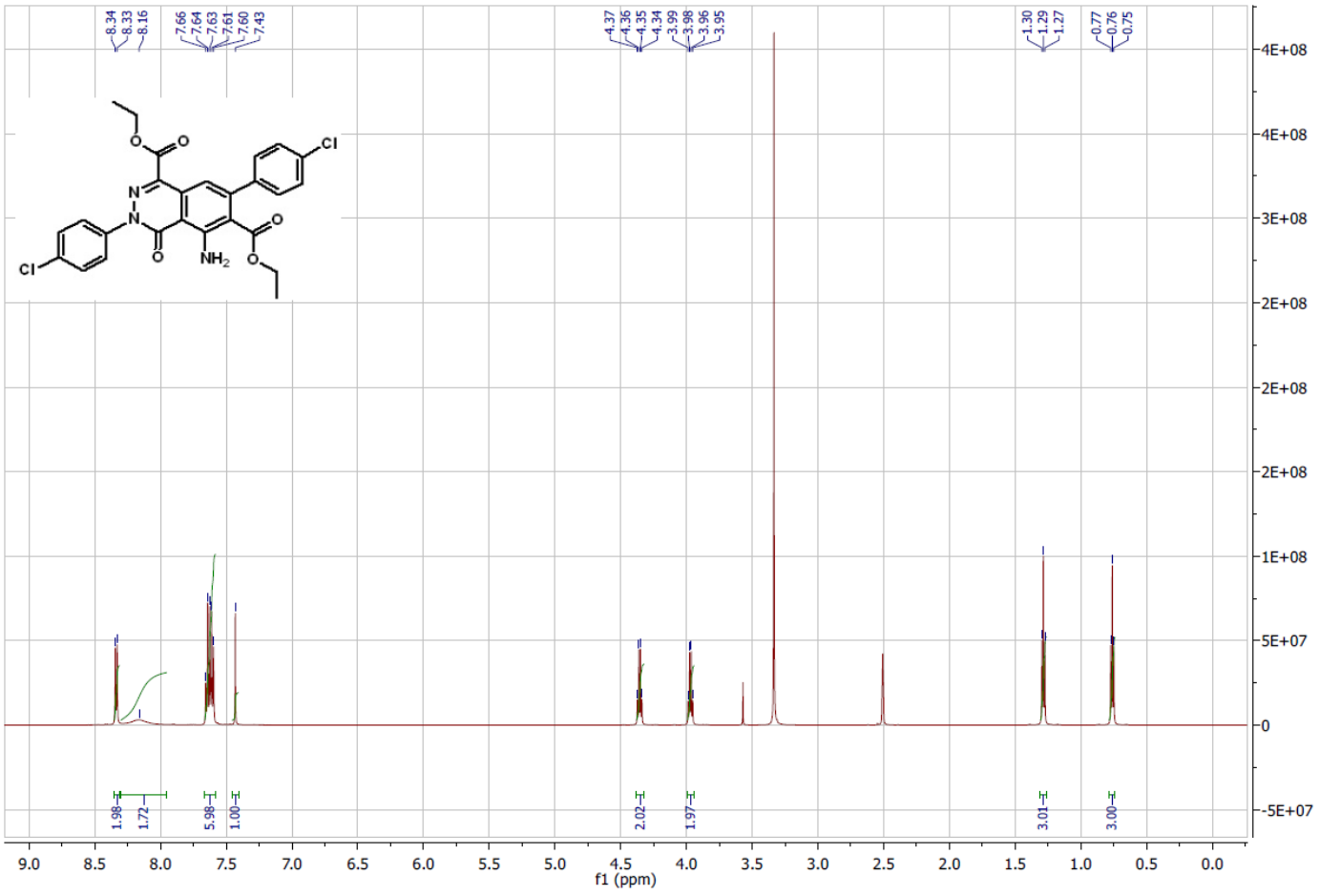

Figure 1. ^{1}H NMR spectrum of compound **3a**.

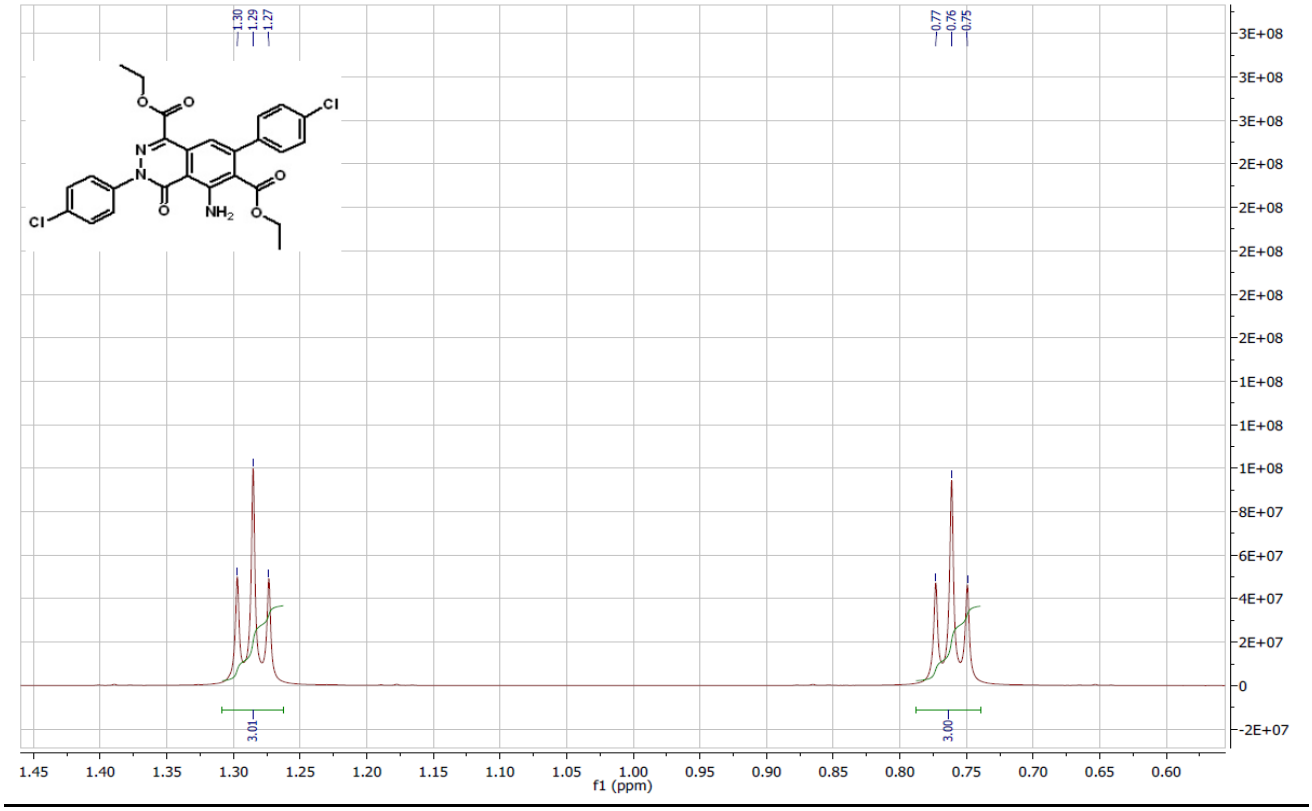

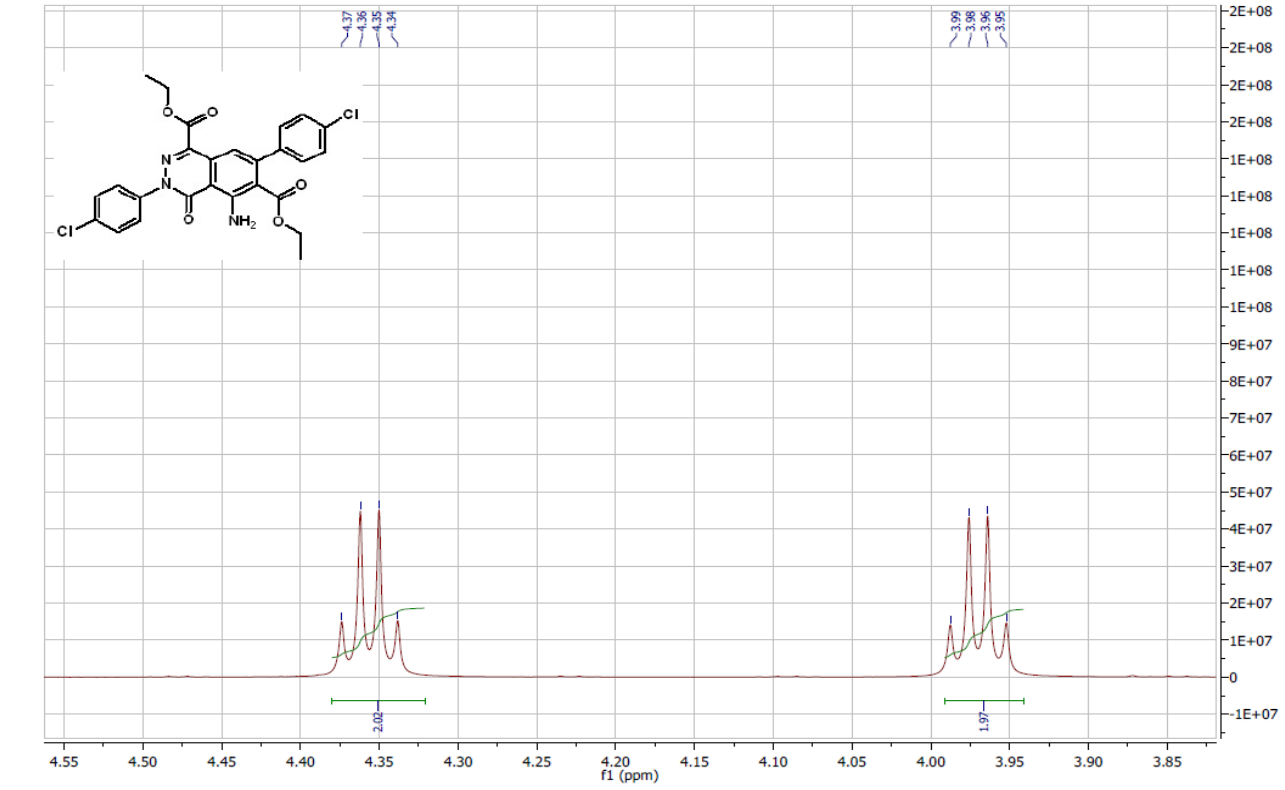

Figure 2. Expanded ^{1}H NMR of compound **3a**.

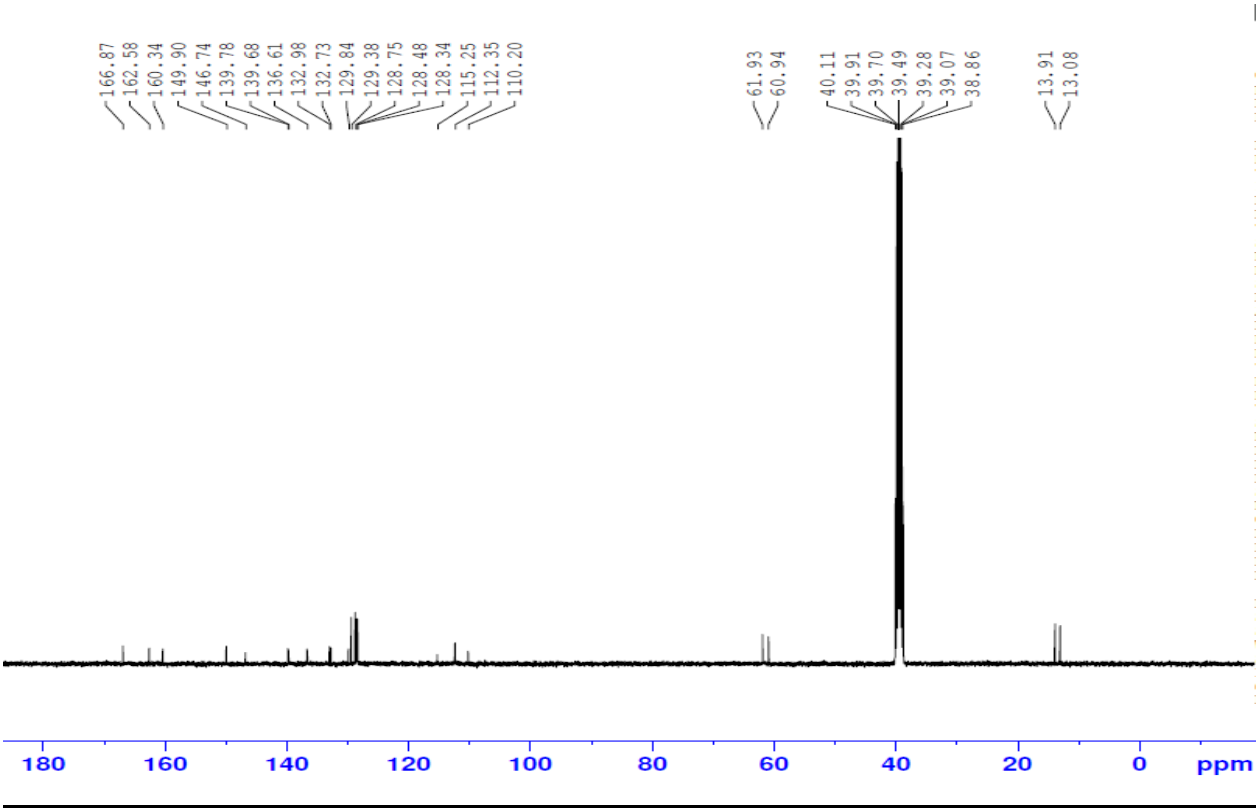

Figure 3. ^{13}C NMR spectrum of compound **3a**.

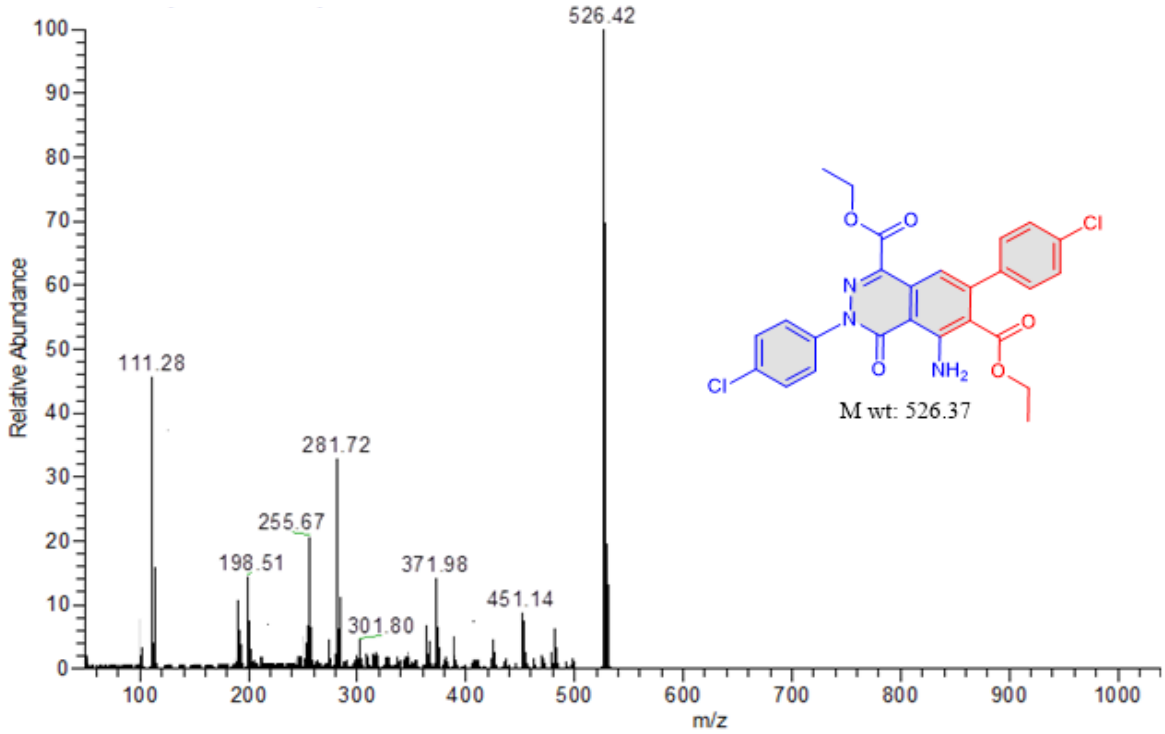

Figure 4. Mass spectrum of compound **3a**.

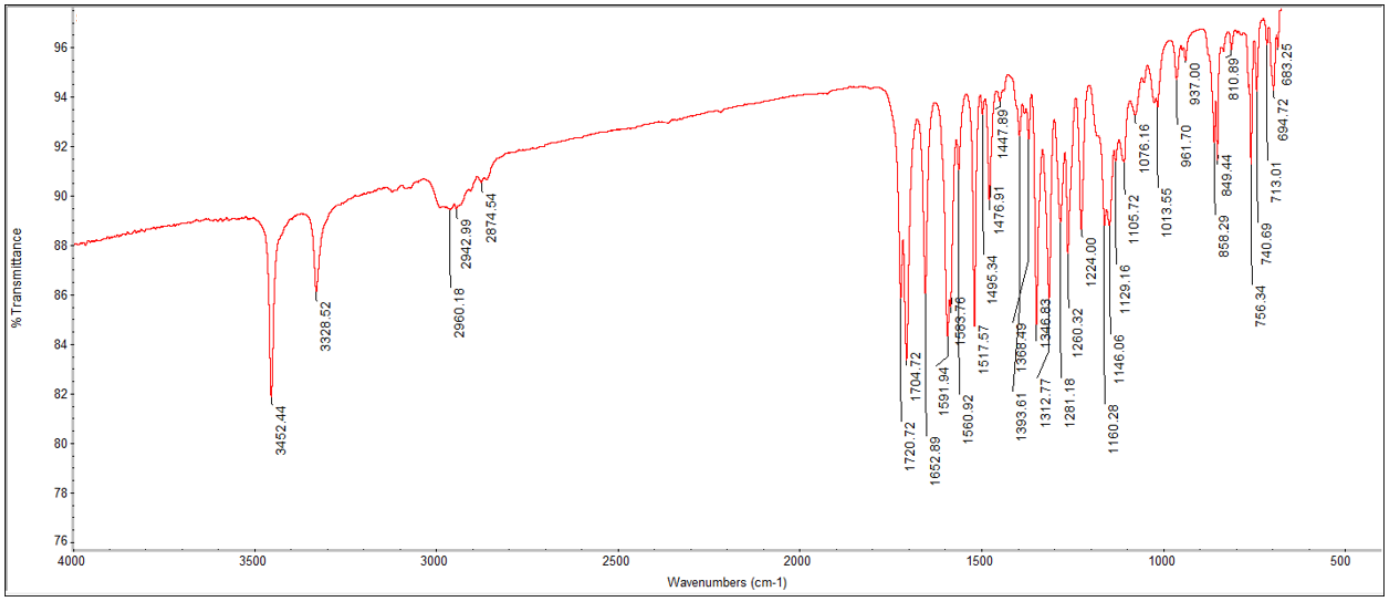

Figure 5. IR spectrum of compound **3a**.

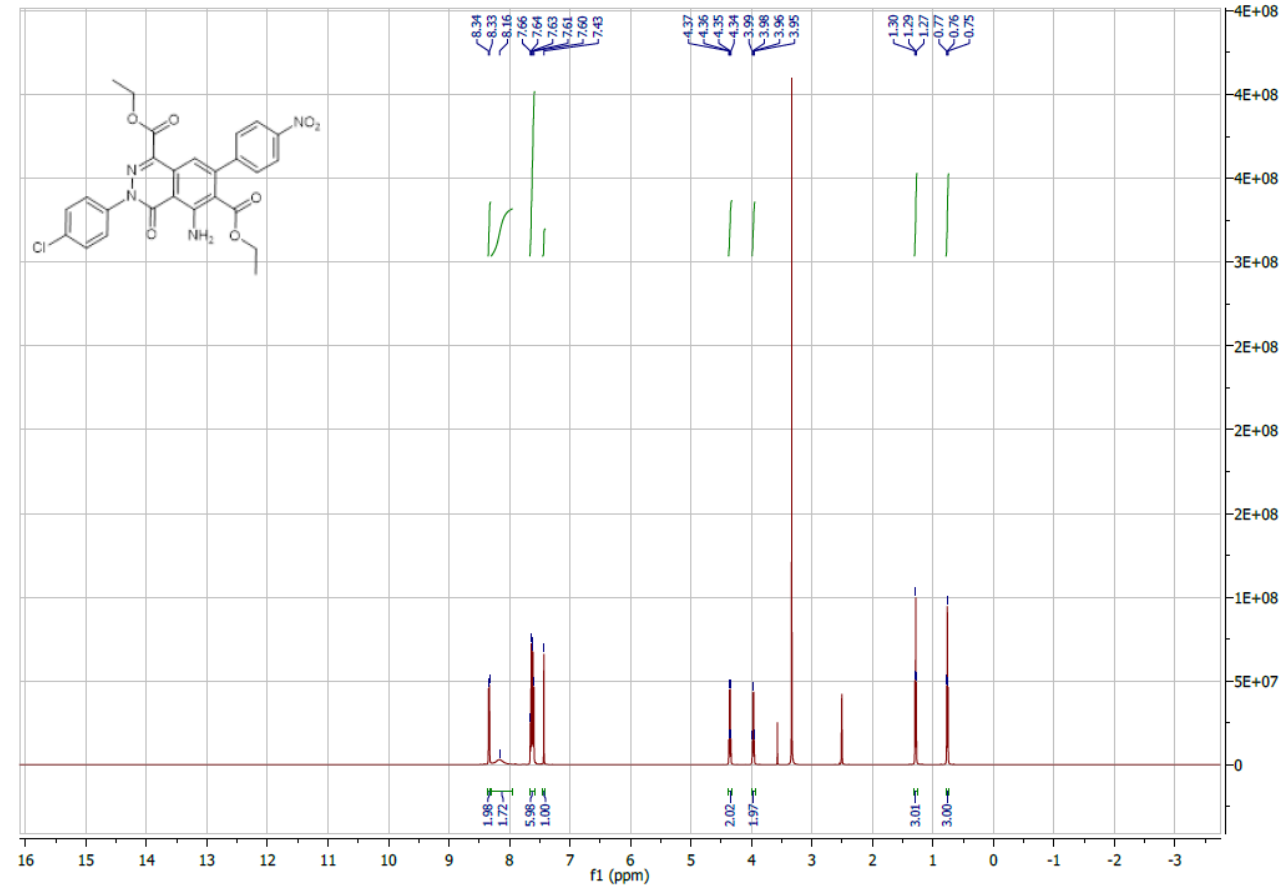

Figure 6. ^{1}H NMR spectrum of compound **3b**.

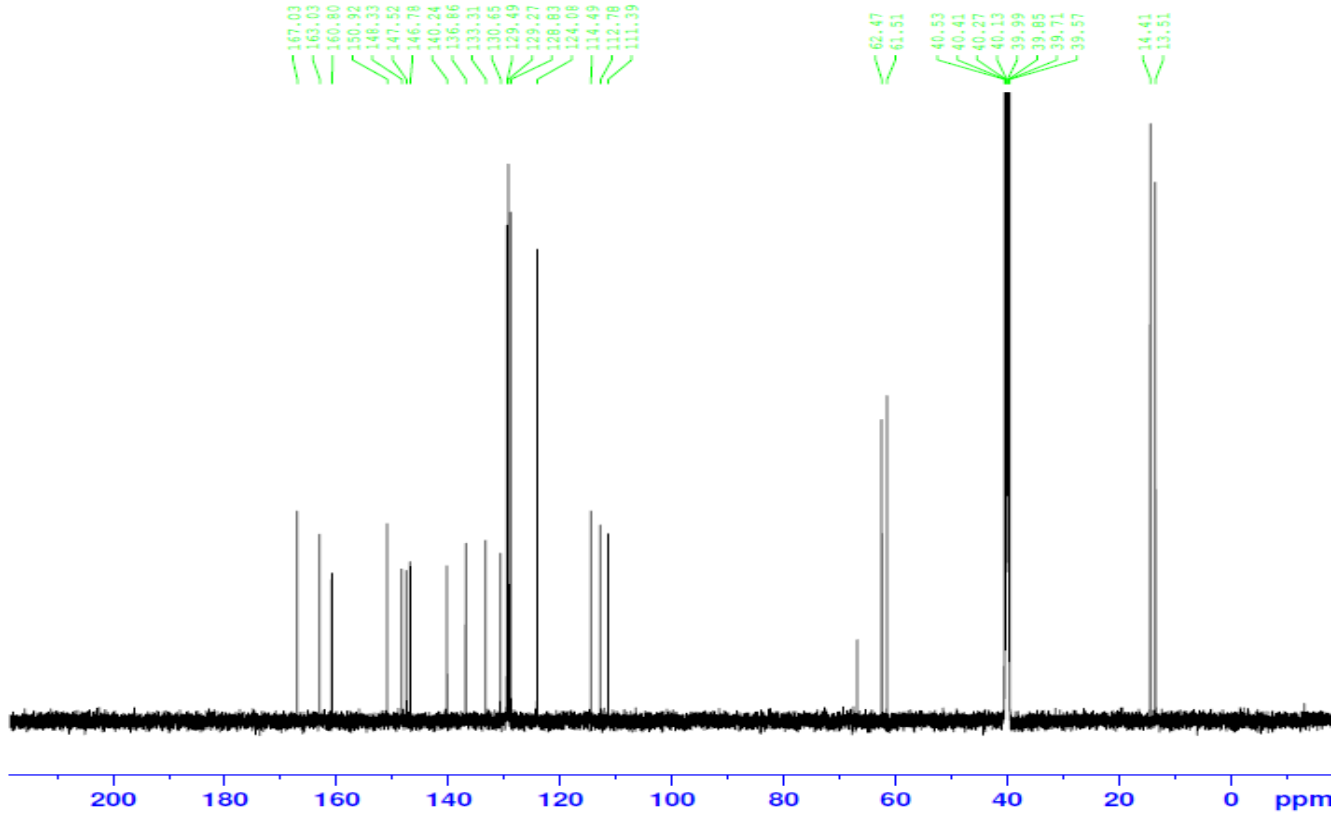

Figure 7. ^{13}C NMR spectrum of compound **3b**.

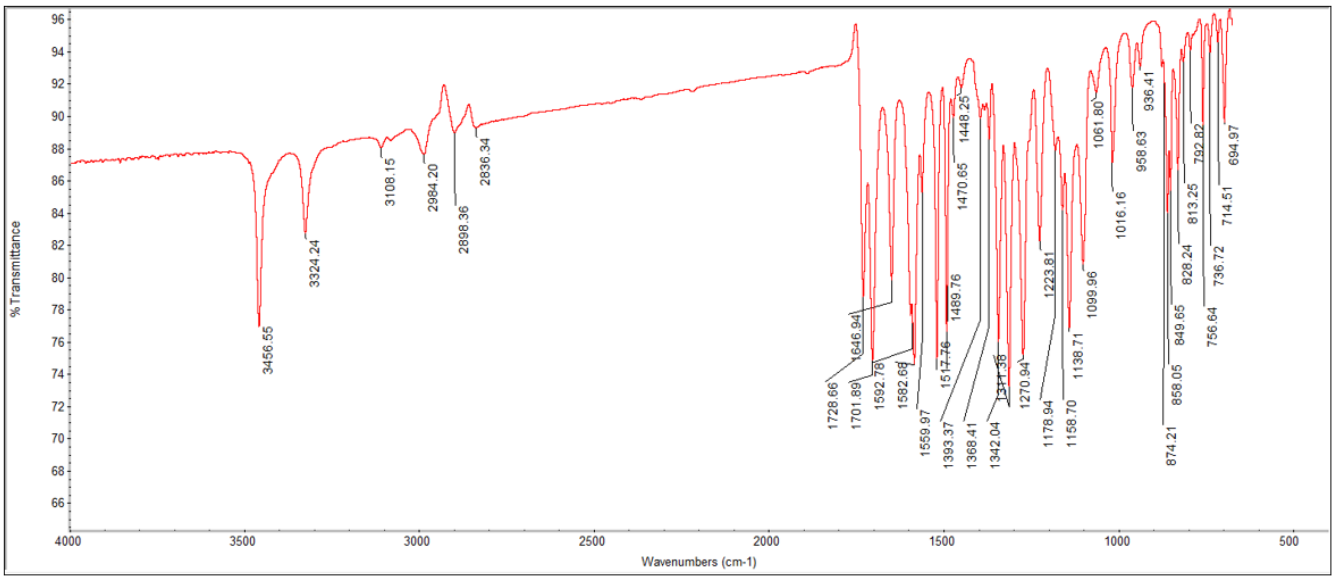

Figure 8. IR spectrum of compound **3b**.

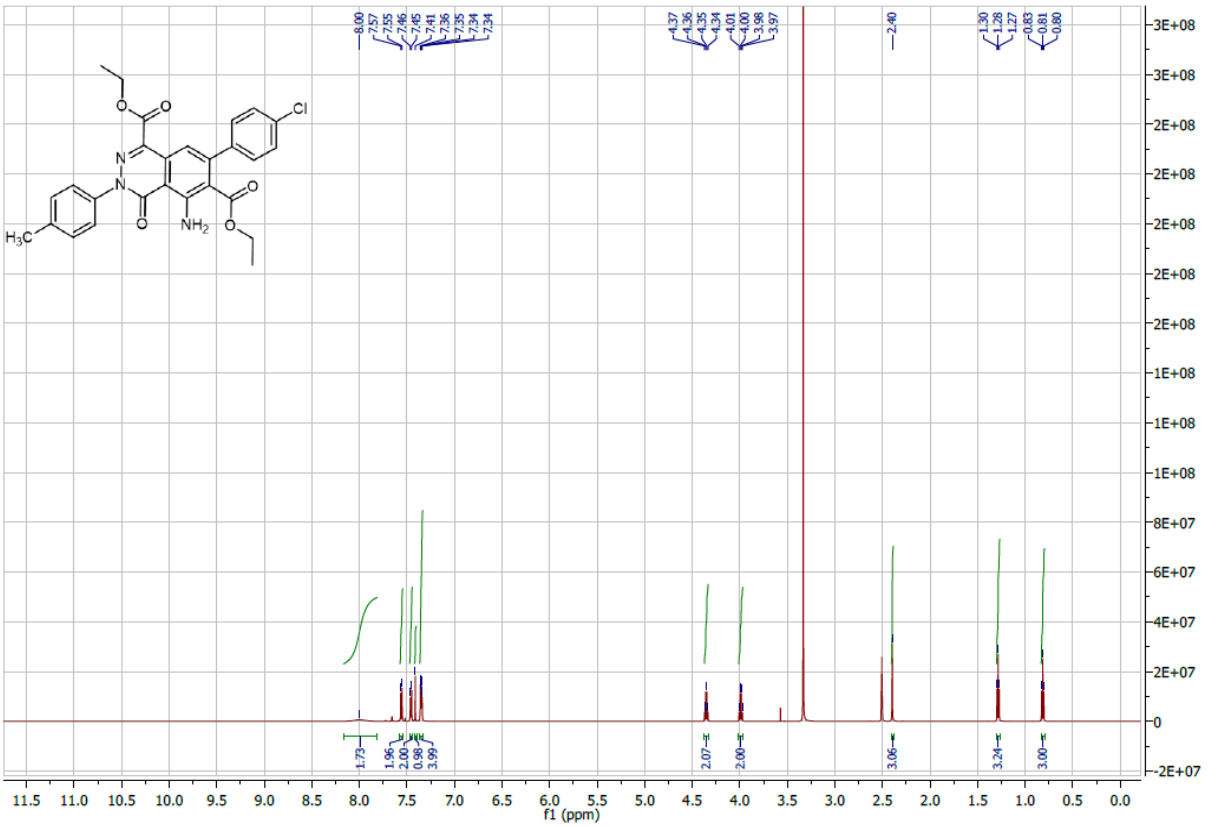

Figure 9. ^{1}H NMR spectrum of compound **3c**.

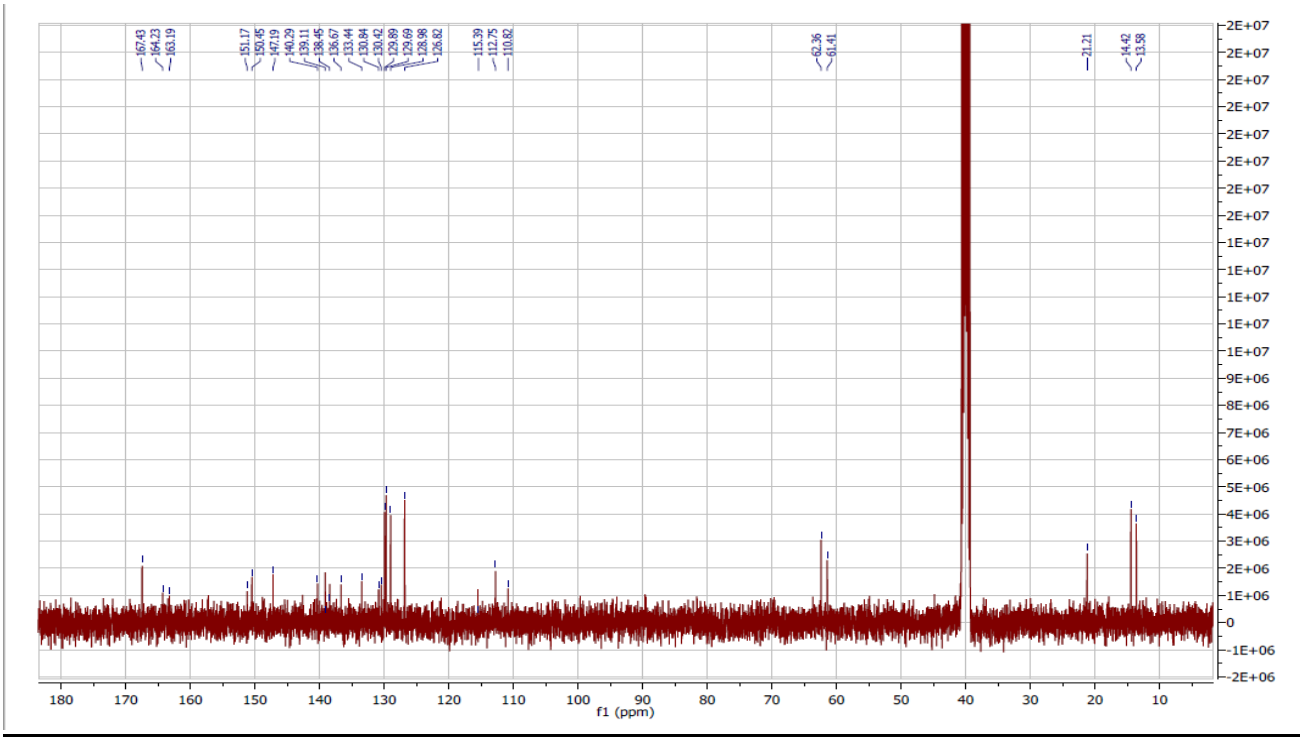

Figure 10. ^{13}C NMR spectrum of compound **3c**.

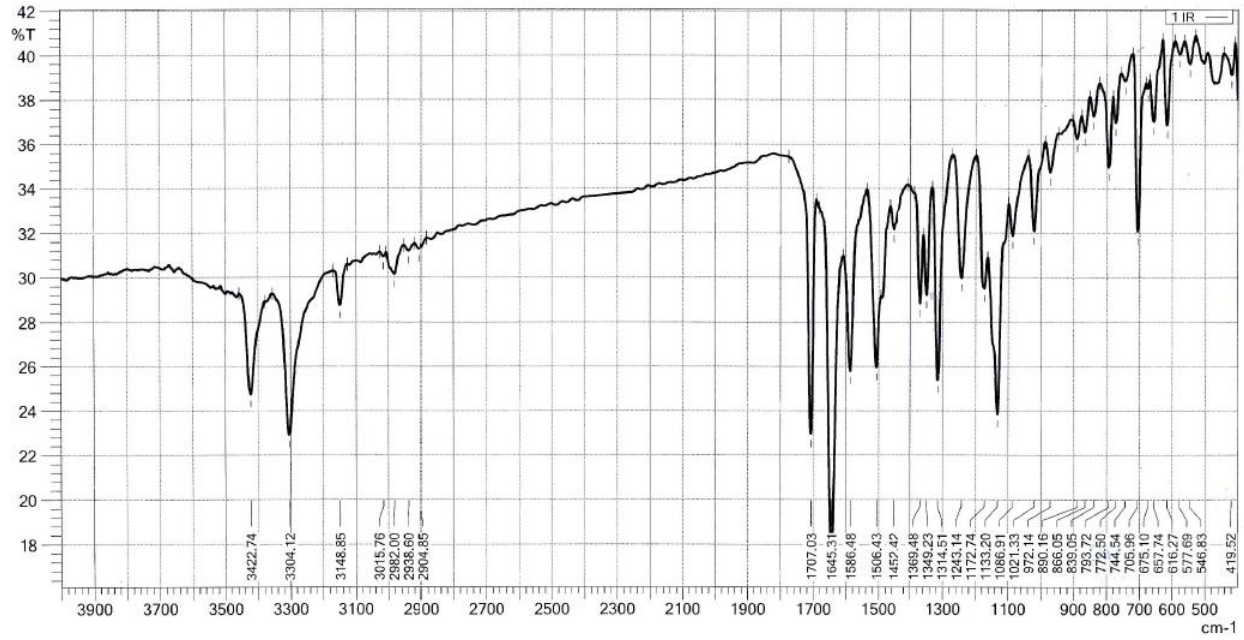

Figure 11. IR spectrum of compound **3c**.

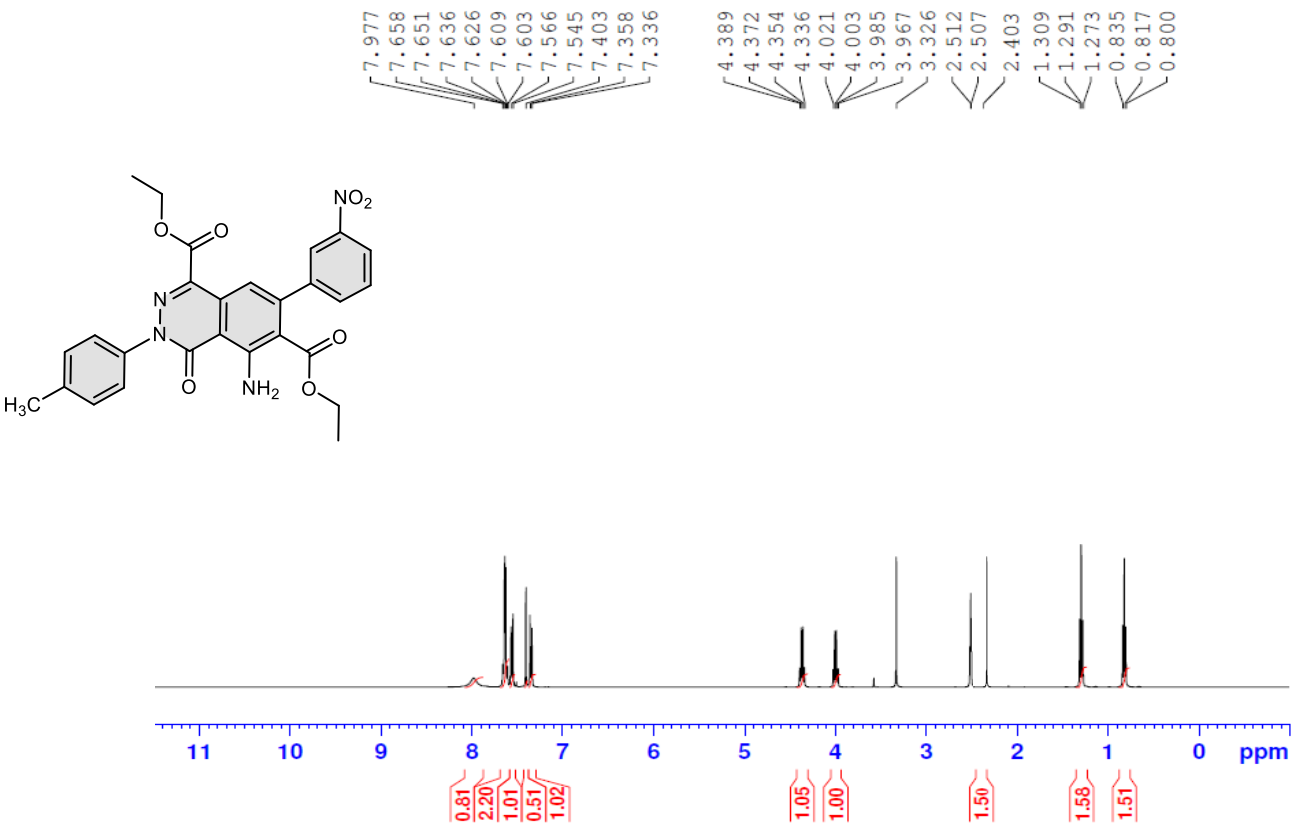

Figure 12. ^{1}H NMR spectrum of compound **3d**.

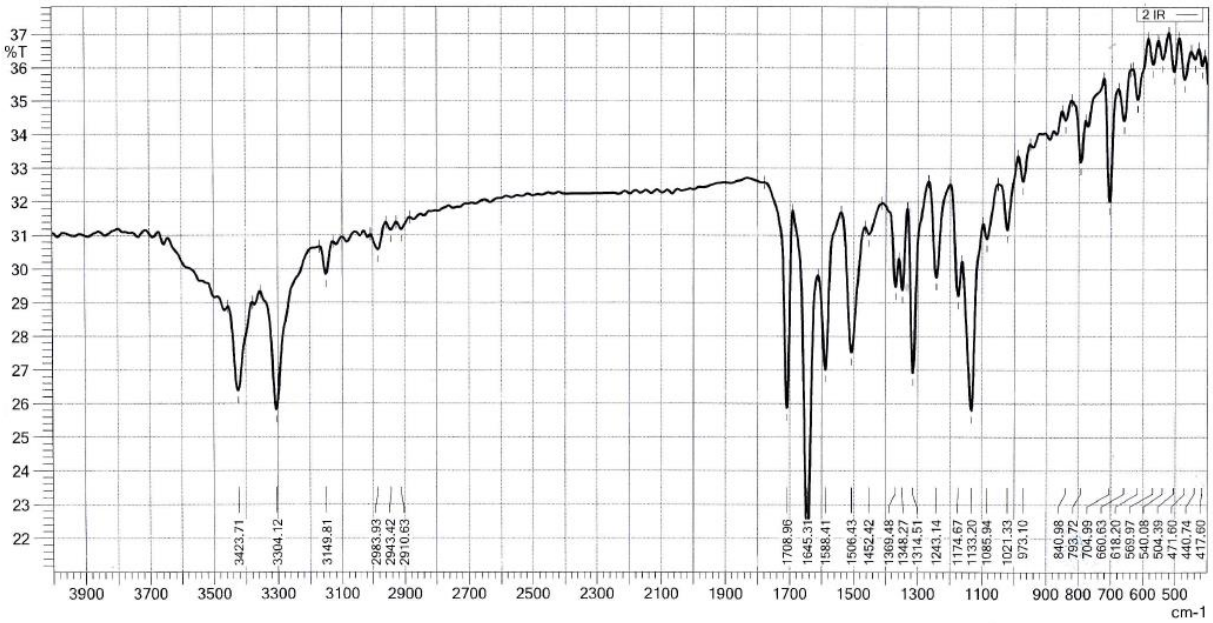

Figure 13. IR spectrum of compound **3d**.

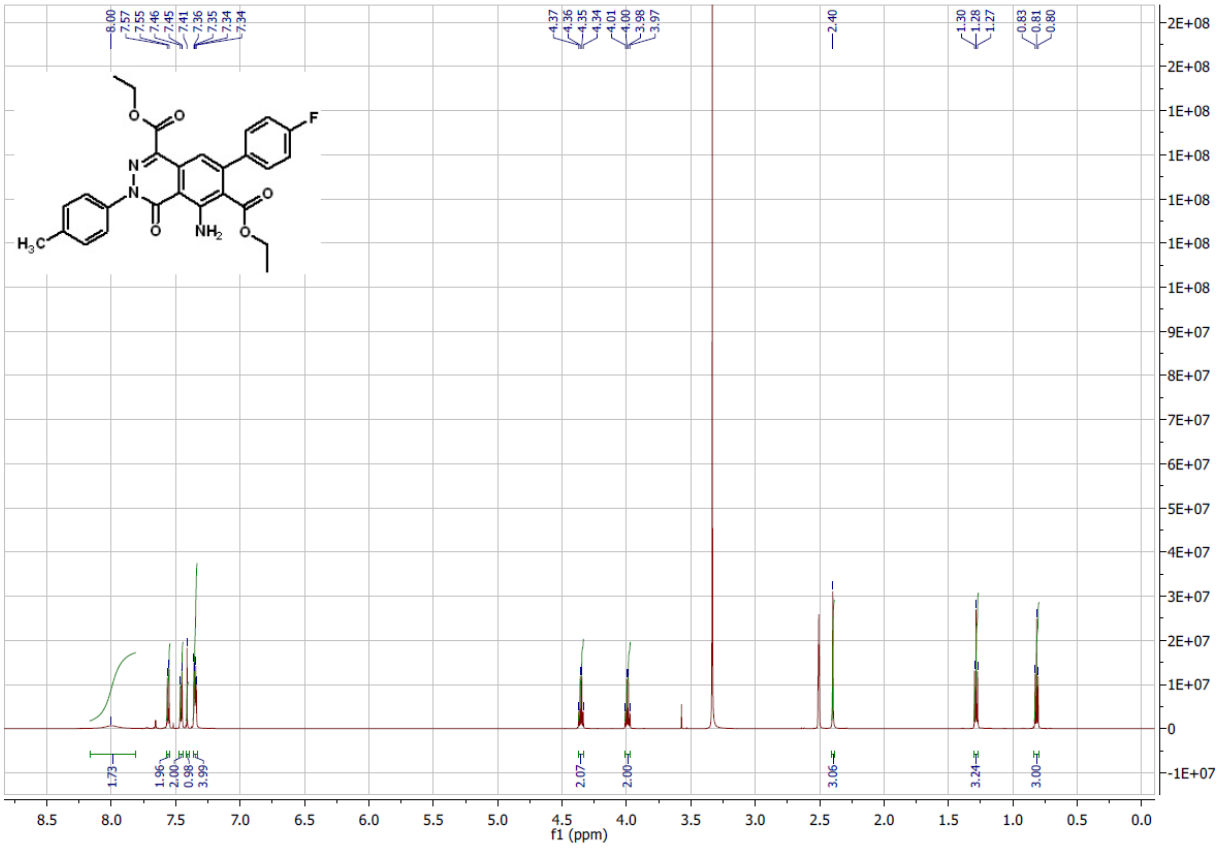

Figure 14. ^{1}H NMR spectrum of compound **3e**.

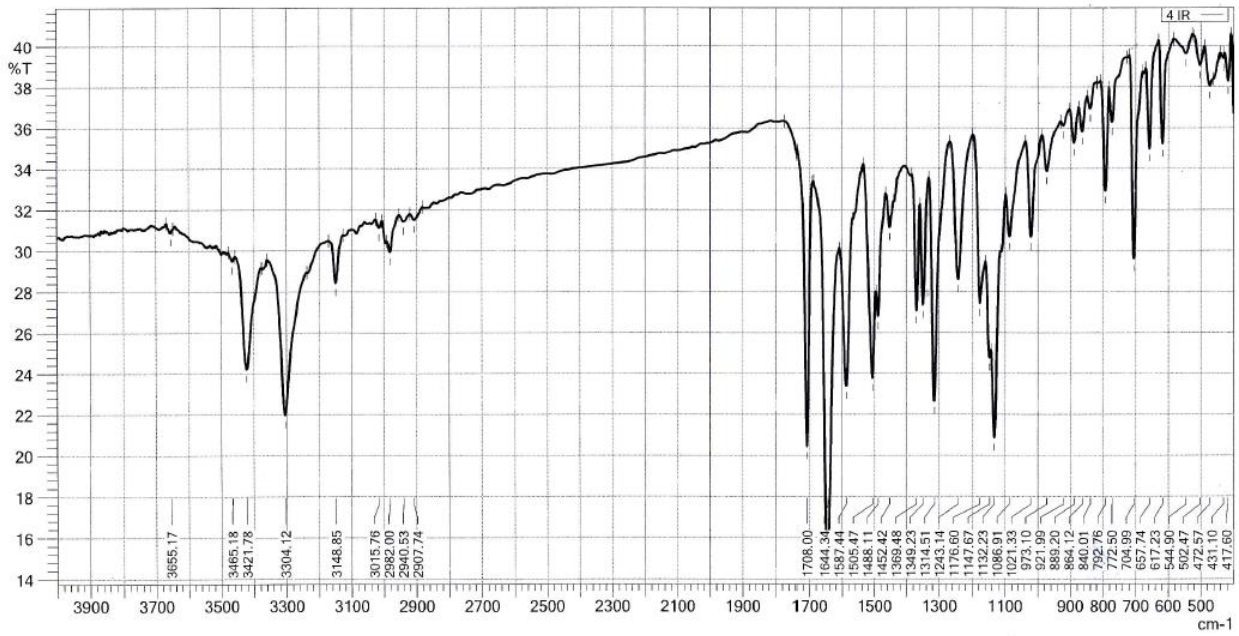

Figure 15. IR spectrum of compound **3e**.

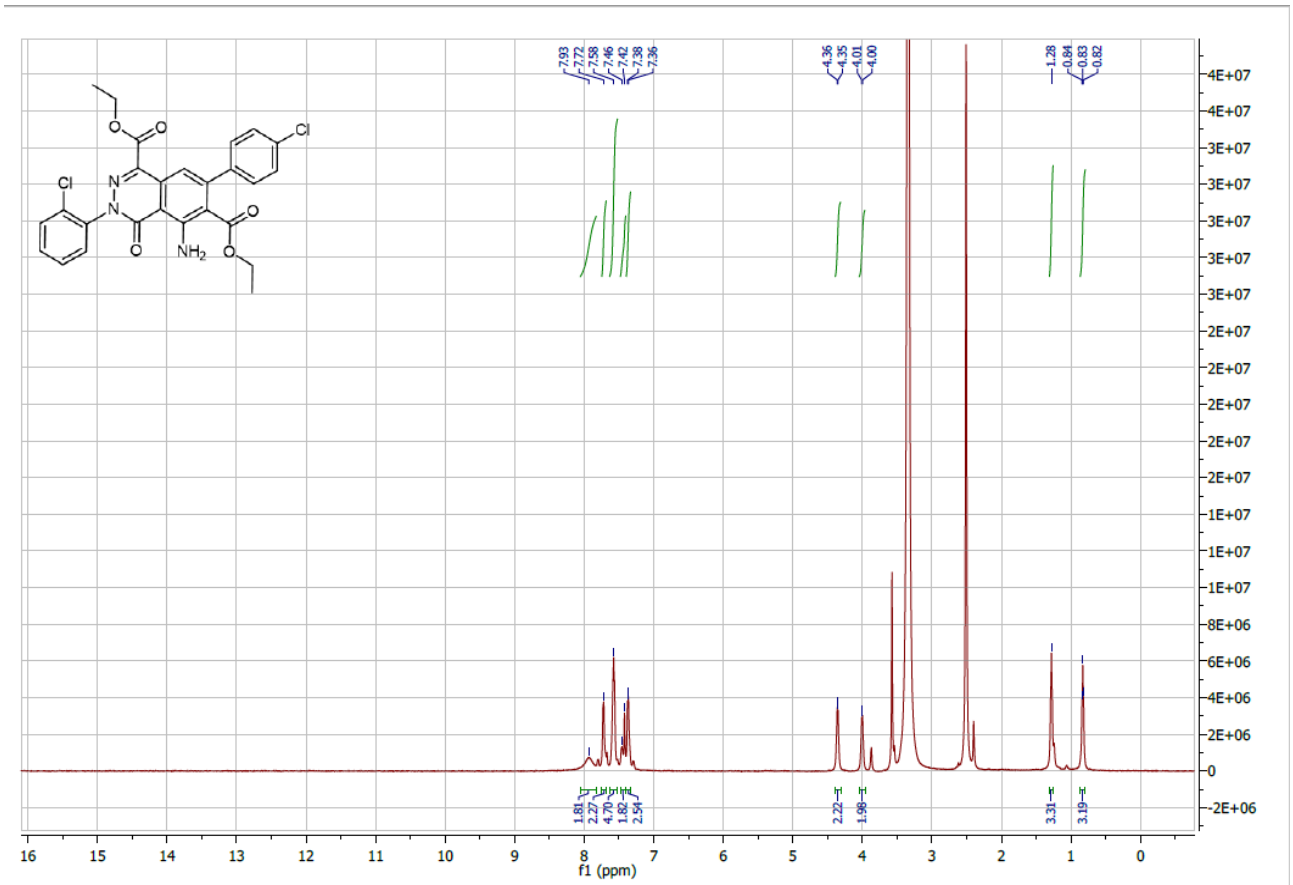

Figure 16. ^{1}H NMR spectrum of compound **3f**.

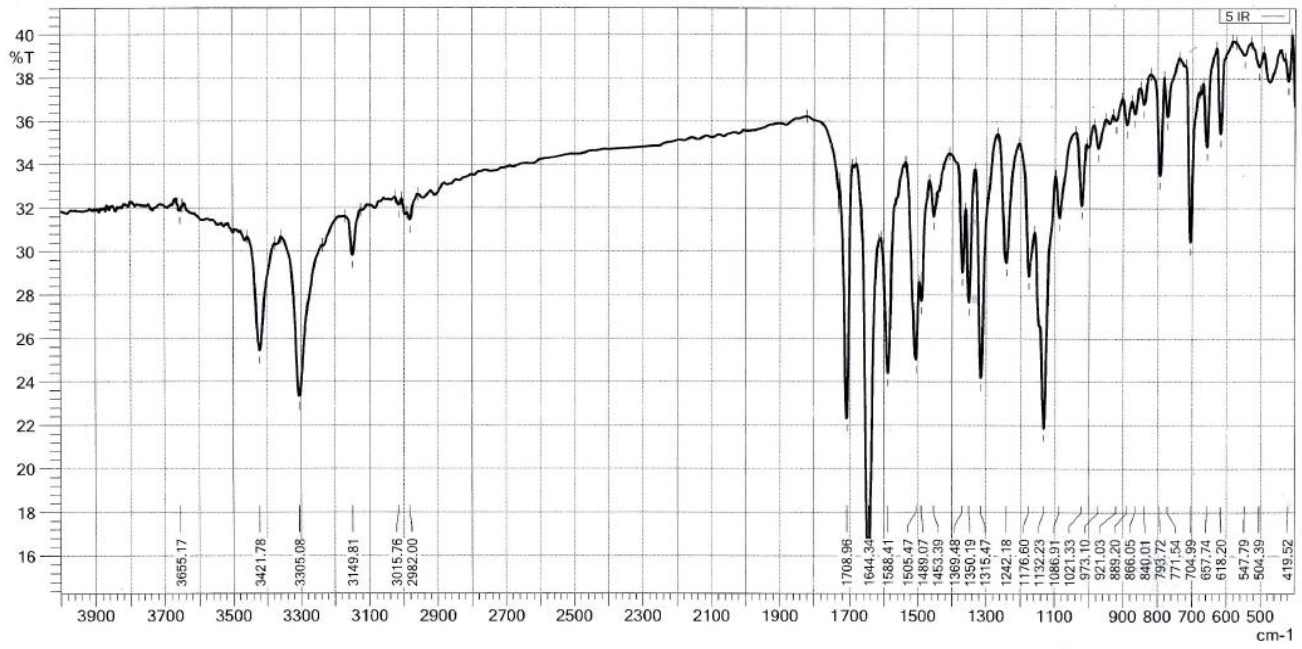

Figure 17. IR spectrum of compound **3f**.

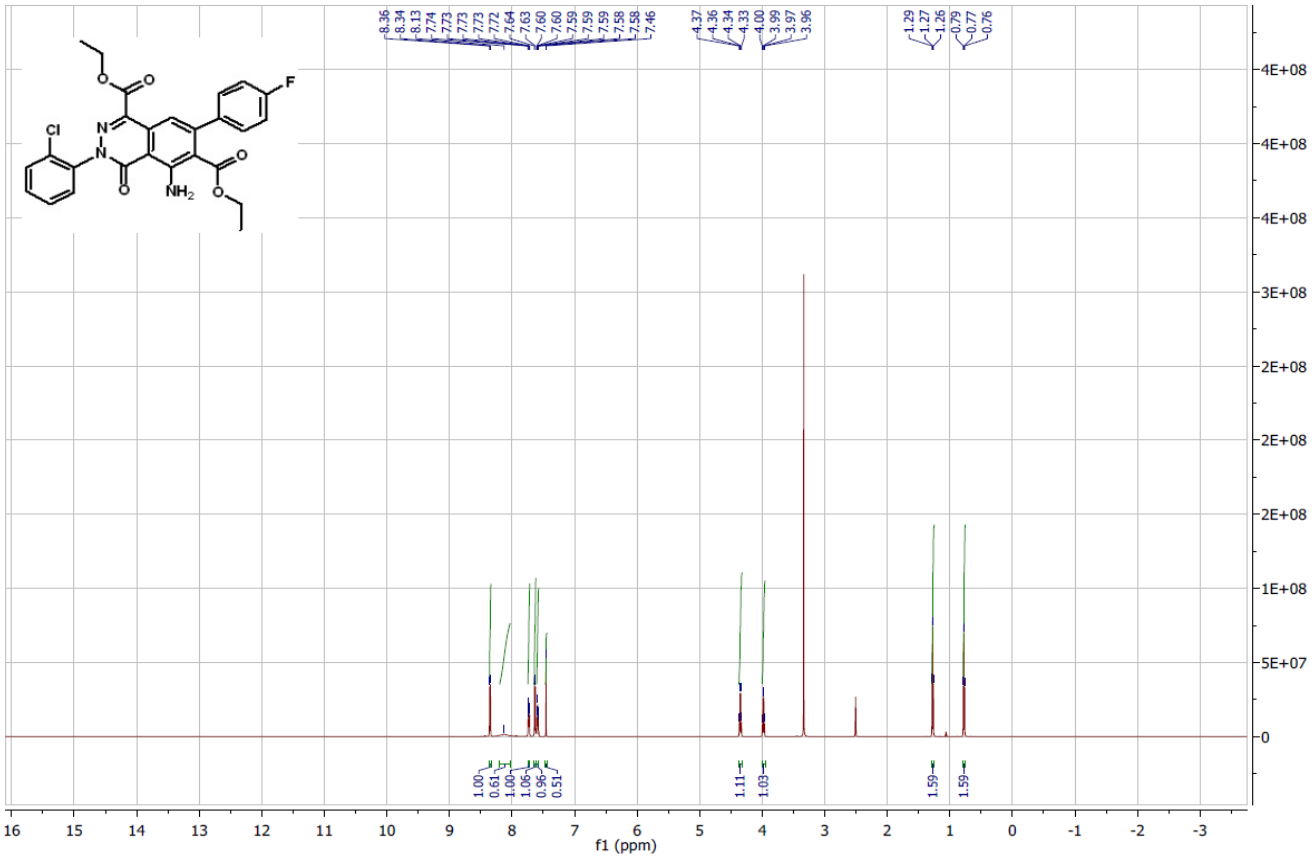

Figure 18. ^{1}H NMR spectrum of compound **3g**.

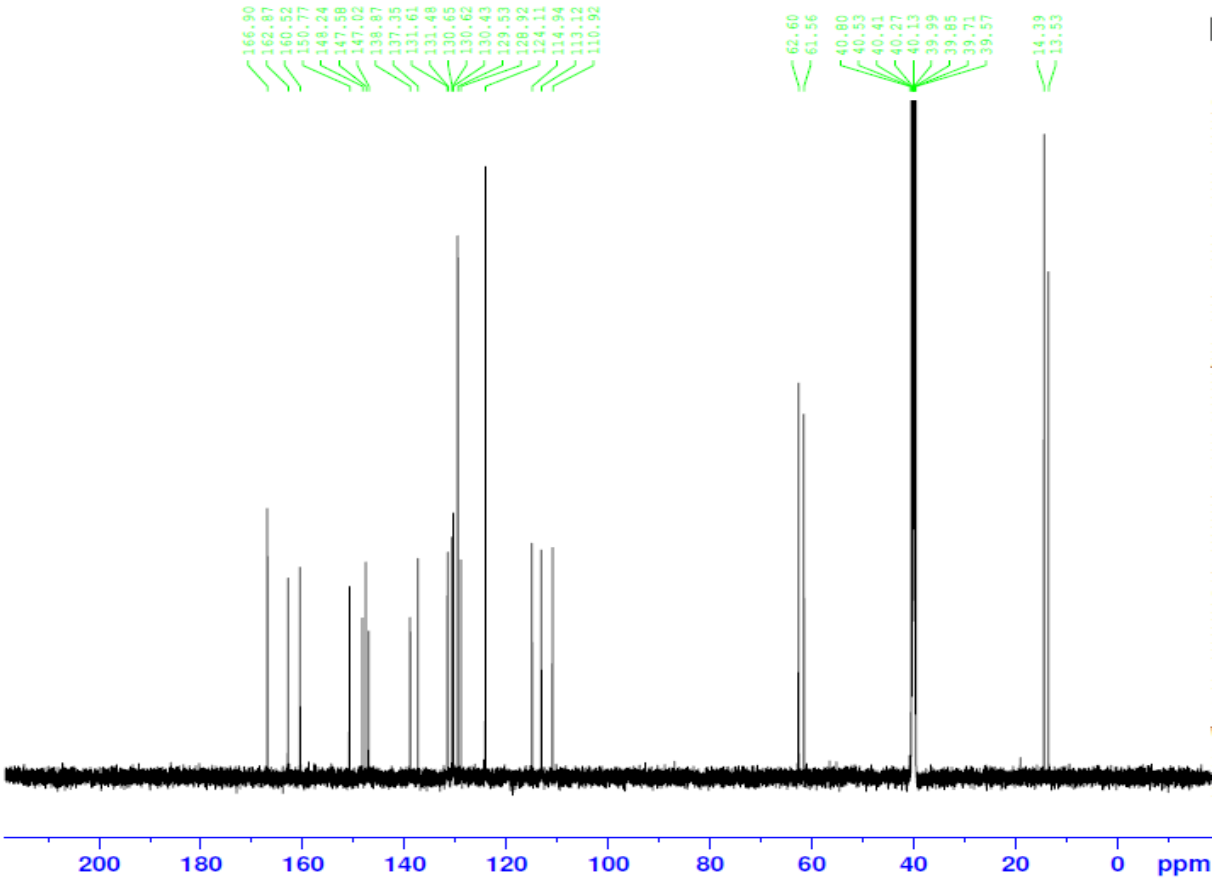

Figure 19. ^{13}C NMR spectrum of compound **3g**.

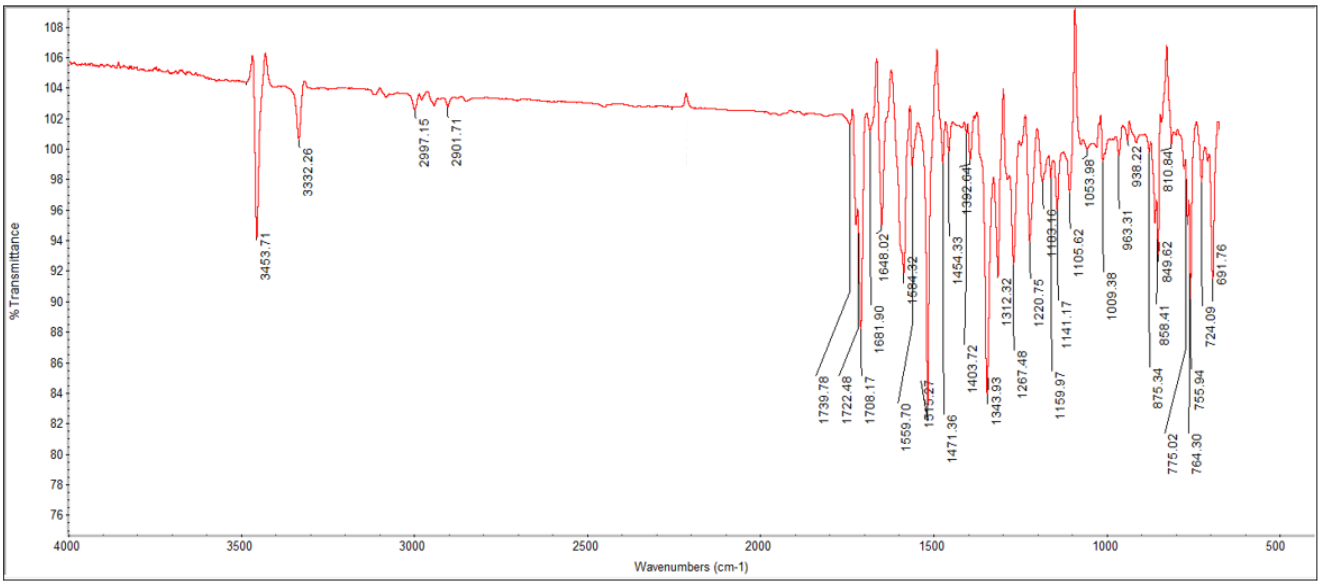

Figure 20. IR spectrum of compound **3g**.

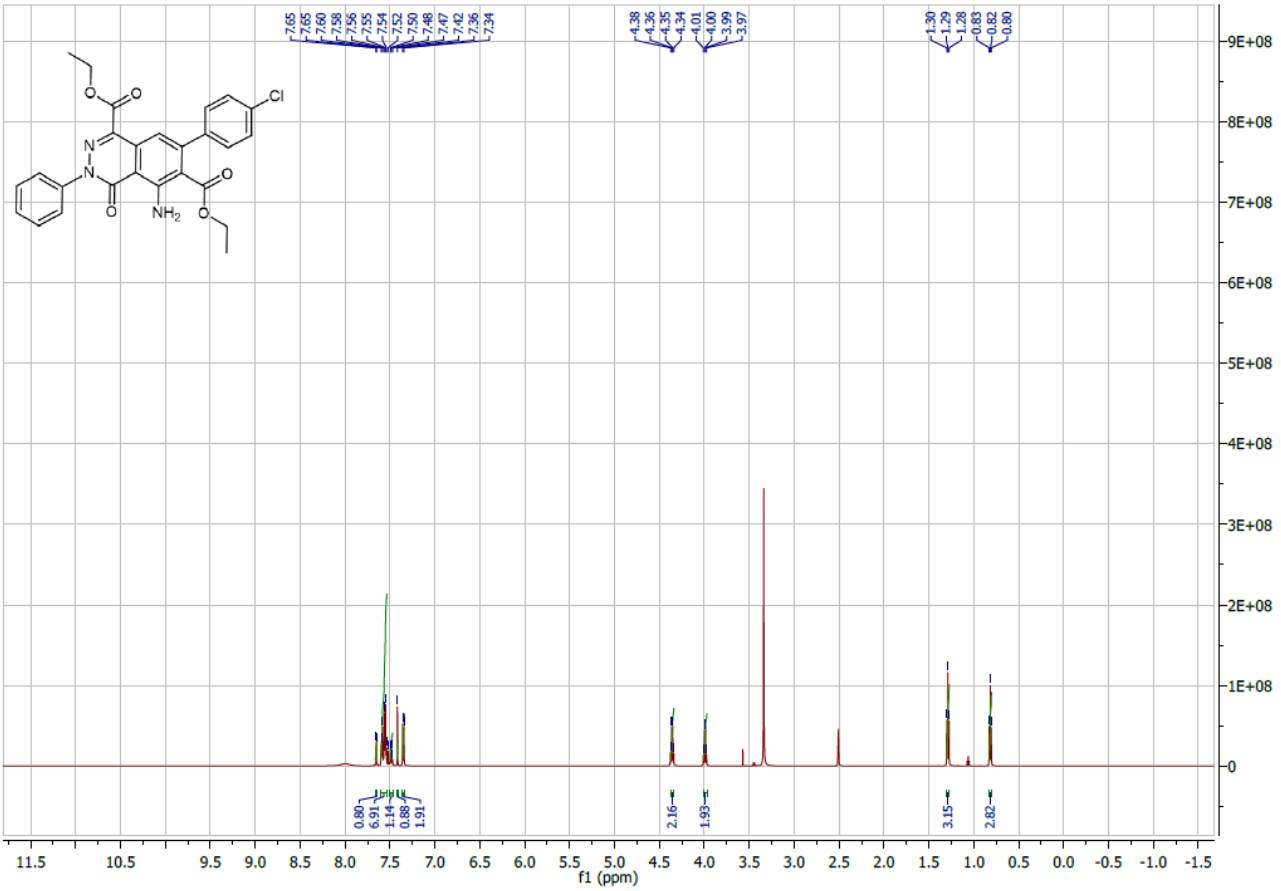

Figure 21. ^{1}H NMR spectrum of compound **3h**.

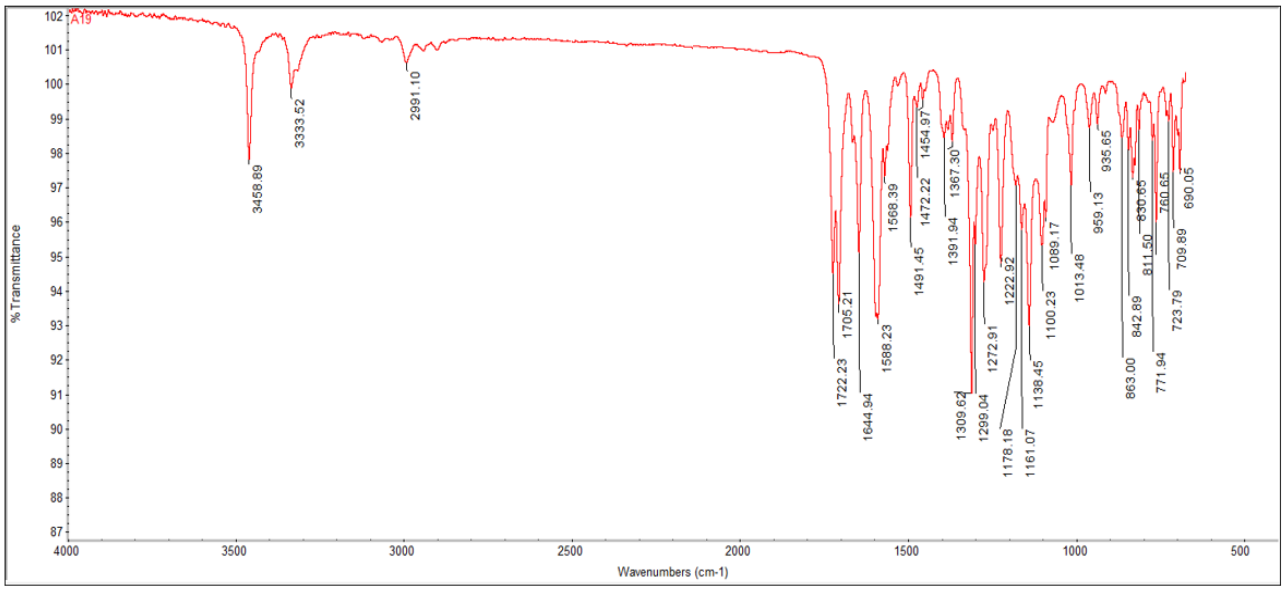

Figure 22. IR spectrum of compound **3h**.

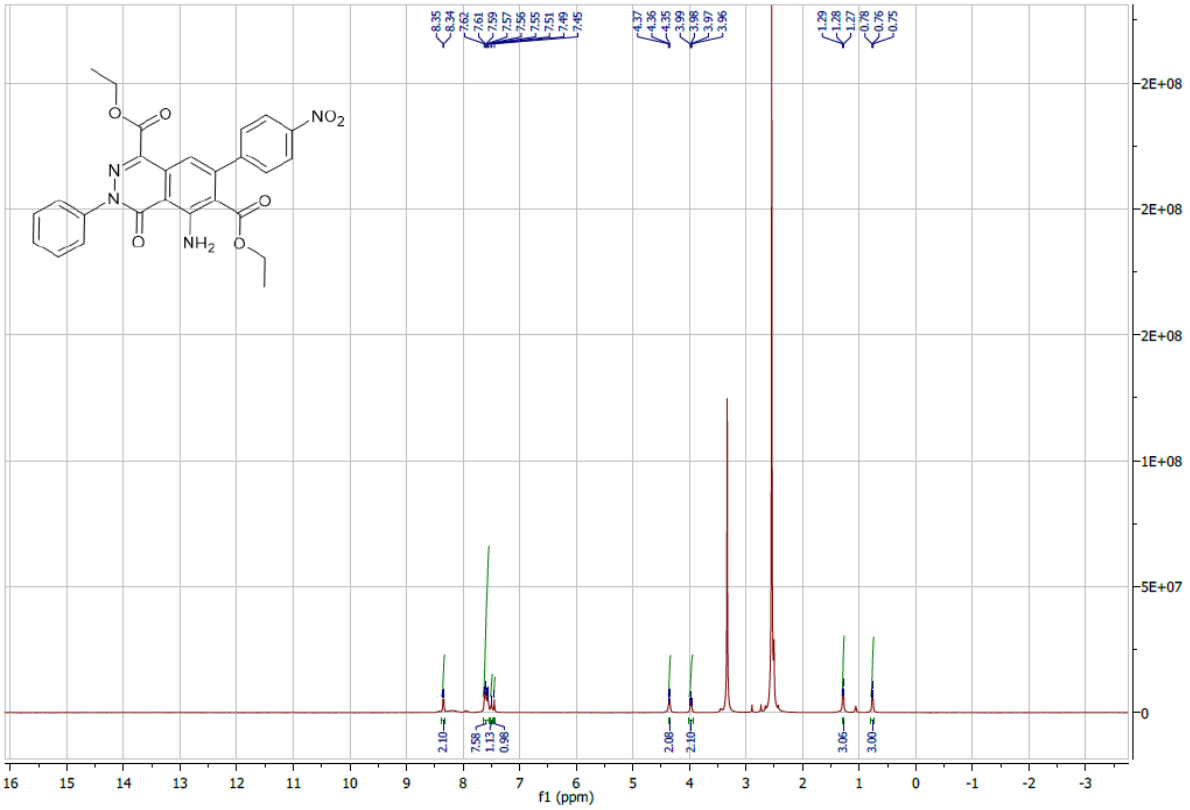

Figure 23. ^{1}H NMR spectrum of compound **3i**.

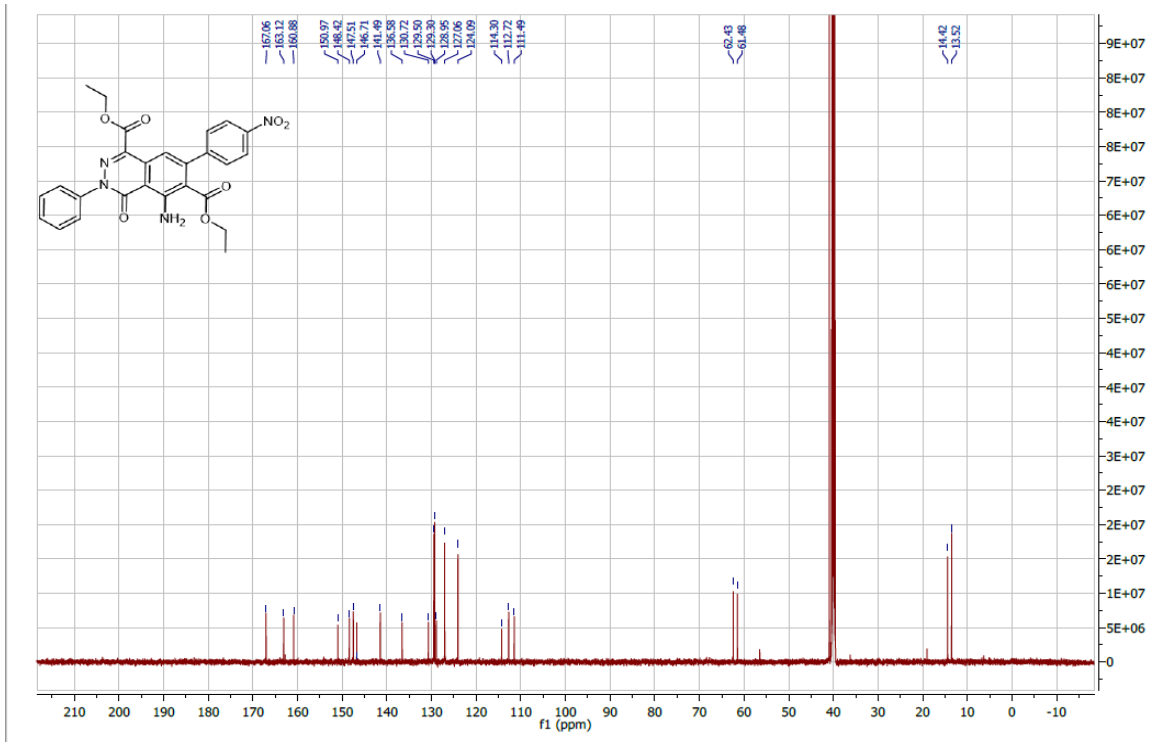

Figure 24. ^{13}C NMR spectrum of compound **3i**.

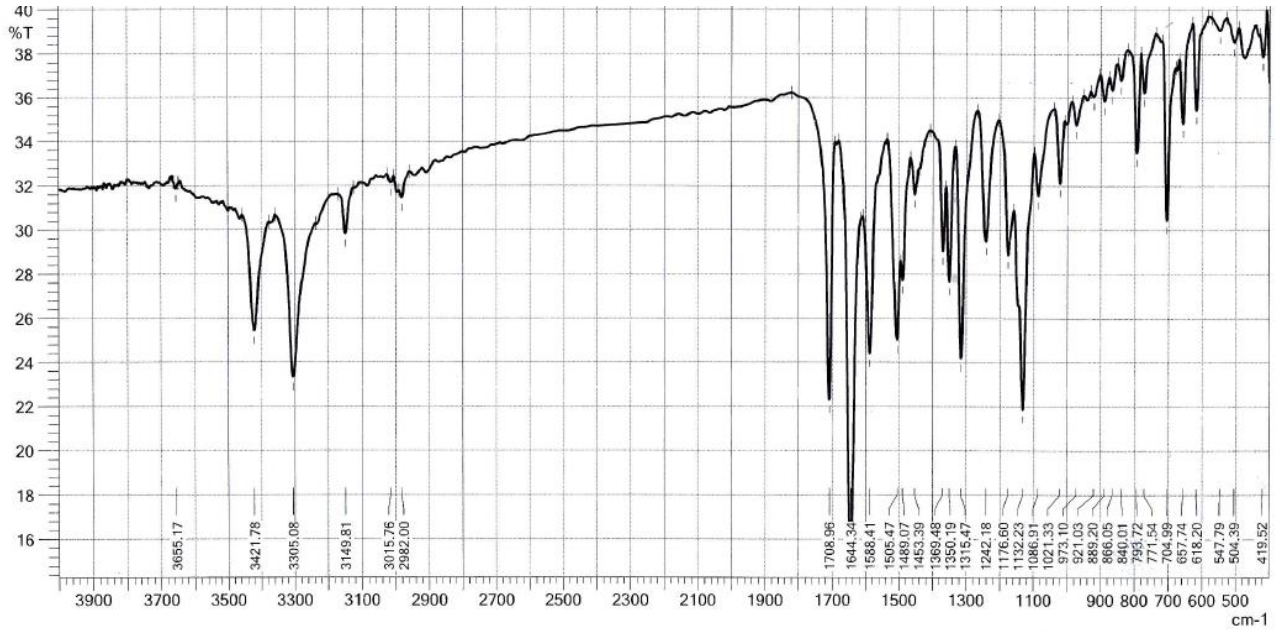

Figure 25. IR spectrum of compound **3i**.

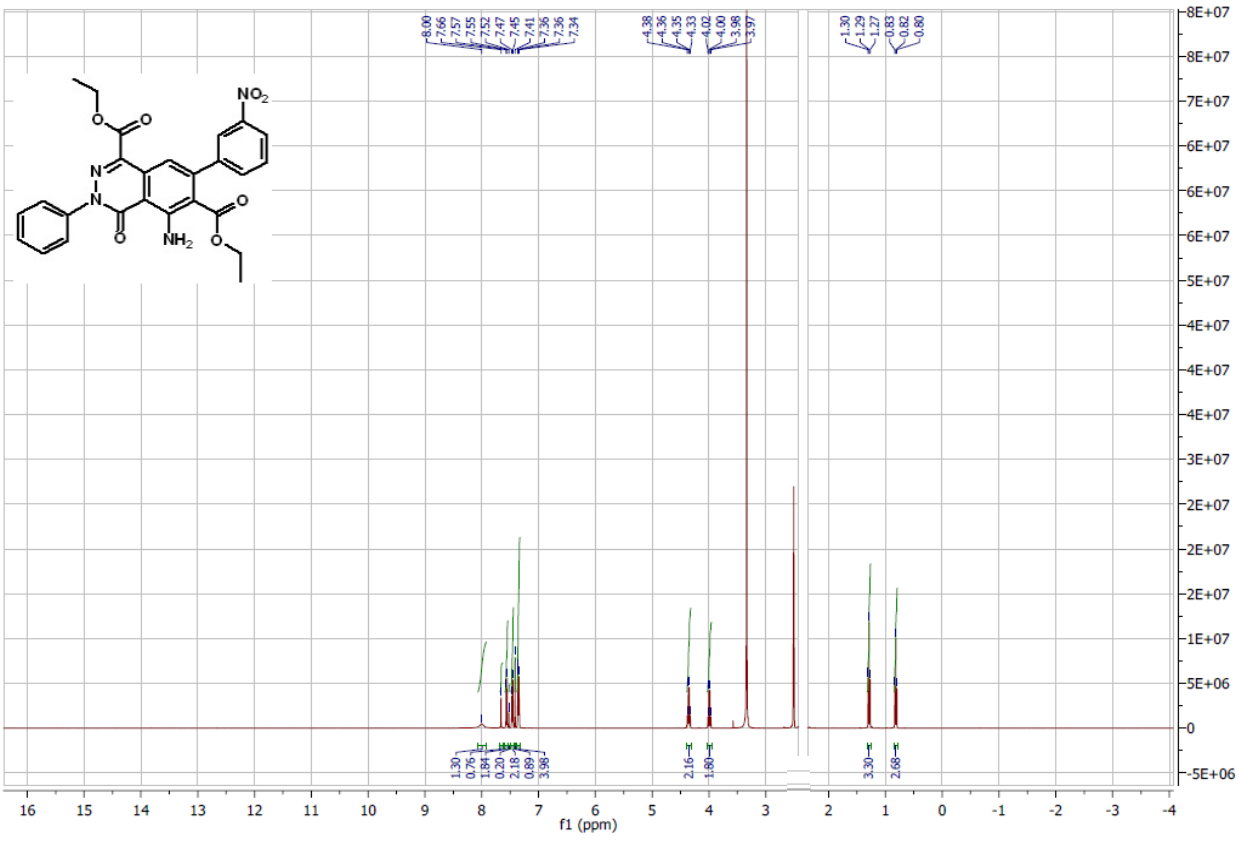

Figure 26. ^{1}H NMR spectrum of compound **3j**.

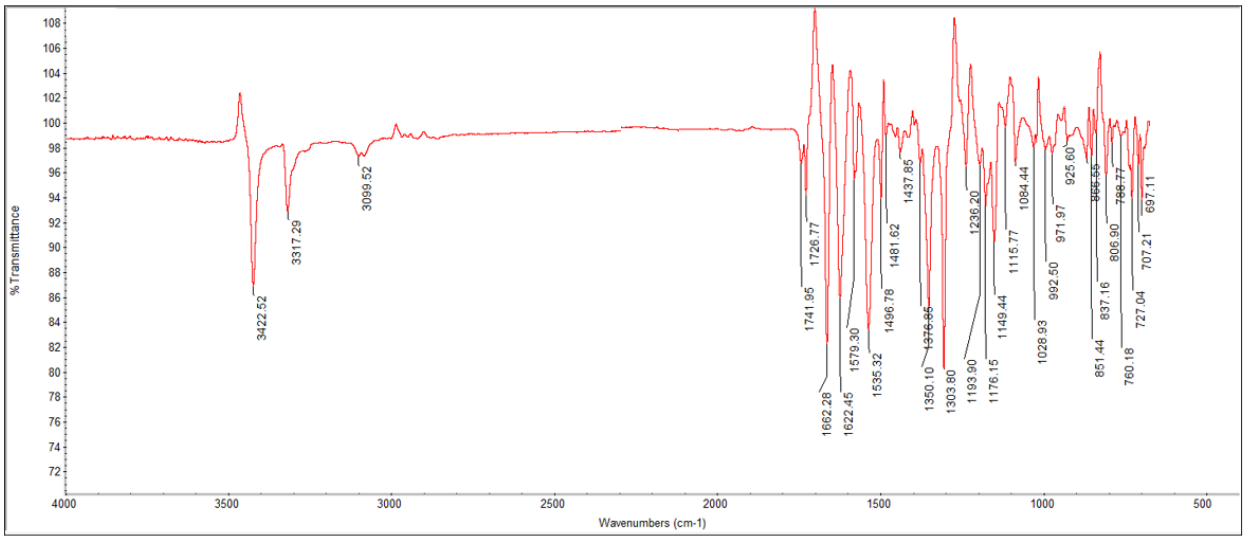

Figure 27. IR spectrum of compound **3j**.

3. References

1. O'Toole, G.A. Microtiter Dish Biofilm Formation Assay. *J. Vis. Exp.* **2011**, e2437, doi:10.3791/2437.
2. Frisch, M.J. *et al*. Gaussian 09, Revision A.02, Gaussian, Inc., Wallingford CT, 2016.
3. Zhurko, G.; Zhurko, D. ChemCraft 1.8, 2005. http:// www.Chemcraftprog.Com.
4. Humphrey, W.; Dalke, A.; Schulten, K. VMD: Visual Molecular Dynamics. *J. Mol. Graph.* **1996**, *14*, 33–38, doi:10.1016/0263-7855(96)00018-5.
5. Grossman, E.F.; Daramola, D.A.; Botte, G.G. Comparing B3LYP and B97 Dispersion-corrected Functionals for Studying Adsorption and Vibrational Spectra in Nitrogen Reduction. *ChemistryOpen* **2021**, *10*, 316–326, doi:10.1002/open.202000158.
6. Sayed, D.S. El; Abdelrehim, E.-S.M. Spectroscopic Details on the Molecular Structure of Pyrimidine-2-thiones Heterocyclic Compounds: Computational and Antiviral Activity against the Main Protease Enzyme of SARS-CoV-2. *BMC Chem.* **2022**, *16*, 82, doi:10.1186/s13065-022-00881-3.
7. Han, C.; Zhang, D.; Xia, S.; Zhang, Y. Accurate Prediction of NMR Chemical Shifts: Integrating DFT Calculations with Three-Dimensional Graph Neural Networks. *J. Chem. Theory Comput.* **2024**, *20*, 5250–5258, doi:10.1021/acs.jctc.4c00422.
8. Lu, T.; Chen, F. Multiwfn: A Multifunctional Wavefunction Analyzer. *J. Comput. Chem.* **2012**, *33*, 580–592, doi:10.1002/jcc.22885.
9. El Sayed, D.S.; Khalil, T.E.; Elbadawy, H.A. Rational and Experimental Investigation of Antihypotensive Midodrine-Fe(III) Complex: Synthesis, Spectroscopy, DFT, Biological Activity and Molecular Docking. *J. Mol. Struct.* **2024**, *1311*, 138421, doi:10.1016/j.molstruc.2024.138421.
10. El-Sayed, D.S.; Sinha, L.; Soayed, A.A. Experimental and Theoretical Quantum Chemical Studies of 2-(2-Acetamidophenyl)-2-Oxo-N-(Pyridin-2-Ylmethyl)Acetamide and Its Copper(II) Complex: Molecular Docking Simulation of the Designed Coordinated Ligand with Insulin-like Growth Factor-1 Receptor (IG. *BMC Chem.* **2024**, *18*, 112, doi:10.1186/s13065-024-01217-z.
11. Abdelrehim, E.M.; El-Sayed, D.S. A New Synthesis of Poly Heterocyclic Compounds Containing [1,2,4]Triazolo and [1,2,3,4]Tetrazolo Moieties and Their DFT Study as Expected Anti-Cancer Reagents. *Curr. Org. Synth.* **2020**, *17*, 211–223, doi:10.2174/1570179417666200226092516.
12. Ibraheem, H.H.; Issa, A.A.; El-Sayed, D.S. Structural Behavior and Surface Layer Modification of (E)-N'-((1H-Indol-3-Yl) Methylene)-4-Chlorobenzohydrazide: Spectroscopic, DFT, Biomedical Activity and Molecular Dynamic Simulation against Candida Albicans Receptor. *J. Mol. Struct.* **2024**, *1312*, 138484, doi:10.1016/j.molstruc.2024.138484.
13. El-Sayed, D.S.; Elbadawy, H.A.; Khalil, T.E. Rational Modulation of N and O Binding in Fe(III) Complex Formation Derived from Hydroxychloroquine: Synthesis, Spectroscopic, Computational, and Docking Simulation with Human Thrombin Plasma. *J. Mol. Struct.* **2022**, *1254*, 132268, doi:10.1016/j.molstruc.2021.132268.
14. Eberhardt, J.; Santos-Martins, D.; Tillack, A.F.; Forli, S. AutoDock Vina 1.2.0: New Docking Methods, Expanded Force Field, and Python Bindings. *J. Chem. Inf. Model.* **2021**, *61*, 3891–3898, doi:10.1021/acs.jcim.1c00203.
15. Bax, B.D.; Chan, P.F.; Eggleston, D.S.; Fosberry, A.; Gentry, D.R.; Gorrec, F.; Giordano, I.; Hann, M.M.; Hennessy, A.; Hibbs, M.; et al. Type IIA Topoisomerase Inhibition by a New Class of Antibacterial Agents. *Nature* **2010**, *466*, 935–940, doi:10.1038/nature09197.

16. Strushkevich, N.; Usanov, S.A.; Park, H.-W. Structural Basis of Human CYP51 Inhibition by Antifungal Azoles. *J. Mol. Biol.* **2010**, *397*, 1067–1078, doi:10.1016/j.jmb.2010.01.075.

17. Sarkar, A.; Concilio, S.; Sessa, L.; Marrafino, F.; Piotto, S. Advancements and Novel Approaches in Modified AutoDock Vina Algorithms for Enhanced Molecular Docking. *Results Chem.* **2024**, *7*, 101319, doi:10.1016/j.rechem.2024.101319.